SunQM-3s10: Using {N,n} QM's Eigen n to constitute Asteroid/Kuiper belts, and Solar {N=1..4,n} region's mass density r-distribution and evolution

Yi Cao
Ph.D. in biophysics
e-mail: yicaojob@yahoo.com

Abstract

Asteroid belt is explained as the leftover "ring stain" of the once out-flying ice-rock mixture fragments (driven by the expansion of the ice-evap-line). The cold-KBO of Kuiper belt is explained as the "ring stain" of the current out-flying methane-ice mixture fragments (driven by the expansion of methane-evap-line, or the solar wind stop line). Using the normalized radial probability function r^2 * |R(n,*l*=n-1)|^2 = [r/r_n * exp(1 - r/r_n)]^(2*n), we calculated out that (at the normalized probability ≥ 0.1), Asteroid belt at {1,8//6} = {0,48//6} has a probability peak at n = 48, with the peak range = 2.7 ±0.6 AU, and Kuiper belt at {3,1//6} = {0,192//6} has a probability peak at n = 192, with the peak range = 43 ±5 AU. Using θ-dimension probability formula [sin(θ)]^[2(n-1)] ≥ 0.01, we calculated out that the n=48 belt has the collective orbits' inclination range < 17.8 degree, and b=192 belt has the collective orbits' inclination range < 8.9 degree. These calculated results fit to the Asteroid belt's and the cold-KBO's experimental data perfectly. Then we proposed a new concept: "Eigen quantum number n' " is the maximum n' that can describe one orbit space's > 90% mass in a single |nLL> = |n',n'-1,n'-1> QM state. So n=48 and n=192 are the Eigen description for Asteroid belt and the cold-KBO. Using the Eigen n, the four undiscovered {3,n=2..5//6} belts (if they did not form planets) 's r ± Δr and Δθ' ranges are also predicted. Using the Eigen n, the Solar {N=1..4,n//6} region's r-dimensional mass distribution was described by r^2*|R(n,*l*)|^2 either at each n shell level, or at each N super-shell level, or at the level of treating all N super-shells as a single entity. The evolution of r-dimensional mass distribution in Solar system (driven by the expansion of rock-evap-line and ice-evap-line) is discussed. The result suggested that any sub-Eigen n' description for an Eigen QM state will be a low resolution and more broad description, and any above Eigen n' description for an Eigen QM state will be a high resolution but needs many linearly combined QM states.

Introduction

The SunQM series papers [1] ~ {14] have shown that the formation of Solar system (as well as each planet) was governed by its {N,n} QM. In papers SunQM-3s6, -3s7, and -3s8, it has been shown that the formation of planet's and star's (radial) internal structure is governed by the planet's or star's radial QM. In papers SunQM-3s3 and -3s9, it has been shown that the surface mass (atmosphere, or rock, or liquid iron) movement of Sun, Jupiter, Saturn, and Earth, etc., is governed by Star's (or planet's) θφ-2D dimension QM. In paper SunQM-3s4, it has been shown that the formation of ring structures of all planets are also governed by their p{N,n} QM. In current paper, I try to use {N,n} QM and the Eigen radial probability curve to explain Asteroid belt and Kuiper belt in our Solar system. Note: For {N,n//q} QM nomenclature as well as the general notes for {N,n//q} QM model, please see paper SunQM-1 section VII. Note: Microsoft Excel's number format is often used in this paper, for example: x^2 = x^2, 3.4E+12 = 3.4*10^{12}, 5.6E-9 = 5.6*10^{-9}. Note: The reading sequence for SunQM series papers is: SunQM-1, 1s1, 1s2, 1s3, 2, 3, 3s1, 3s2, 3s6, 3s7, 3s8, 3s3, 3s9, and 3s4. Note: For all papers of SunQM series, reader should check "SunQM-4s1: Updates and Q/A for SunQM series papers" for the most recent updates and corrections.

I. Using {N,n//q} QM structure to explain how Asteroid belt and Kuiper belt were formed

From wiki "Kuiper belt", "*While many asteroids are composed primarily of rock and metal, most Kuiper belt objects are composed largely of frozen volatiles (termed "ices"), such as methane, ammonia and water*". Asteroid belt locates in [1,8//6}o orbit space which is close to {2,1//6} position, and Kuiper belt locates in {2,6//6}o orbit space which is at {3,1//6} position. By comparing the position and composition between Asteroid belt and Kuiper belt, we can learn a lot about how they were formed.

First, let's see the {N,n//q} QM explanation for why Asteroid belt and Kuiper belt were formed. As shown in SunQM-2 Table 6, an n=1 QM state has a complete QM's RF (rotation diffusion, or RotaFusion). In Solar {N,n//6} QM structure, an n=1 orbit shell includes {N-1,n=6..11//6}o orbit spaces. Therefore mass in {N-1,n=6..11//6}o orbit shells is affected by high RF more than that of its neighbors at {N-1,5//6}o , or {N,1//6}o orbit spaces, and this high RF force prevent the mass accretion, so it intended to leave the mass as belt. This explains that why at {1,8//6}o orbit shell, the mass forms Asteroid belt. It also explains that in {2,n=6//6}o orbit shell (or it can be even broader one like {2,n=6..11//6}o orbit shells, or much narrow one like {0,192//6}o orbit shell), the mass forms Kuiper belt. For this reason, in Figure 2 of SunQM-1, in both {1,n=6..11//6}o and {2,n=6..11//6}o orbit shell regions I have assigned higher $\Delta\theta$' variations than their neighbor regions.

Second, let's use the classical physics to explain how Asteroid belt and Kuiper belt were formed. Paper SunQM-1s1 section-VII gives the detailed hypothesis about how Asteroid belt was formed. A summary is given below: About 4.5 billion years ago, during the Solar system formation, a pre-Sun ball quantum collapsed from {6,1} to {0,2}, and it was accompanied by a Hydrogen fusion ball quantum expansion from smaller than {-7,1} to {0,1}. The heat of the {0,1} Hydrogen fusion ball generated a rock-evap-line initially at {1,1} and then expanded first rapidly and then slowly to today's ~{1,2}. It also generated a ice-evap-line initially at {2,1}={1,6} and then expanded rapidly to {1,8} and then slowly to today's ~{1,9}. During this period, large amount of ice (in the form of large or small fragments made of mixture of ice and rock, total about 1.06x of today's Jupiter mass) in the {2,1} spherical space (or, more accurately, in the {1,n=1..5}o orbits spaces) was evaporated and flew outward (or was excited to the higher QM orbit at {2,2} or {2,3}). ~ 80% of this out-flying mass was captured by Jupiter at orbit {2,2}, and the rest ~ 20% was captured by Saturn at orbit {2,3}. This caused Jupiter increased its mass from the original Jupiter (~ 10% of today's mass) to 100% of today's mass, and Saturn increased its mass from the original Saturn (~ 20% of today's mass) to 100% of today's mass. Very small amount of this out-flying mass was captured by Uranus at orbit {2,4}, or by Neptune at orbit {2,5}. There was also tiny amount of this out-flying mass, due to at the low end of the Boltzmann velocity distribution in +r dimension, stopped the out-flying on the way to {2,2} orbit, or in the region of {1,n=6..11//6}o orbit spaces and formed Asteroid belt there afterward.

Then why the Asteroid belt is concentrated in {1,8}o orbit space? It can be explained by the following hypothesis: About 4.5 billion year ago, right after the H-fusion ball quantum expanded its size to {0,1}, the ice-evap-line rapidly expanded to the size of {1,7}, so the low speed out-flying ice-rock mixture fragments within {1,7} were quickly driven outward and concentrated mostly in the {1,7}o (and some in the {1,8}o) orbit space. Then the rapid expansion of ice-evap-line ended and it was replaced by the slow expansion. During the period of slow expansion of ice-evap-line, the Sun-faced ice evaporation on the ice/rock mixture fragments generated weak out-flying force, which was not much stronger than the random directional force generated by the surface ice sublimation of the same ice/rock mixture fragments, so the ice/rocky mixture fragments were slowly moving from {1,7}o orbit space to {1,8}o orbit space. Within probably 0.5 billion years, all ice in the ice/rocky mixture fragments was either evaporated or sublimated, left only rocky fragments mostly in the {1,8}o orbit space (see Figure 1b). So these rocky fragments (now we named it as the Asteroid belt) were trapped in {1,8}o orbit space since ~ 4 billion years ago. Even the ice-evap-line slowly passed {1,9}, these rocky fragments are no longer out-flying because there was no ice to be evaporated to generate out-flying force for them!

The similar explanation can be used to explain how Kuiper belt was formed. This time, the ice-rocky mixture fragments are replaced by the methane-ice mixture fragments. Similar as that in the ice/rock mixture, ice's melting point and boiling point is much lower than that of rock, in the methane/ice mixture, methane's melting point and boiling point is much lower than that of ice. Scientists already showed that the solar wind stops at {3,1//6} (see wiki "Solar wind"). So in the space within {3,1}, solar wind hit the Sun-facing side of the methane-ice mixture fragments and evaporated the surface methane. Through Newton's third low, the evaporated methane provided the force to push the methane-ice mixture fragments further away from the Sun. Beyond {3,1}, the solar wind stops, so the methane evaporation stops, and the methane-ice mixture fragments' out-flying stops. In this way, all methane-ice mixture fragments inside {3,1} space were moved outward and dumped in the {3,1}o orbit space, forming a belt we call it Kuiper belt. So the current Kuiper belt can still be out-moving if

the solar wind stop-line keeps expanding. A few billion year later (or after Sun become a red giant), it is expected that (at least part) of current Kuiper belt's mass will move out further to {2,7}o orbit space or even beyond.

Just like when you drop a water drop on a low-quality dyed cloth, the outward diffusion of the water carries the dye pigment away from the drop center. After dried, a water "ring stain" is left where the dye molecules are transported outward and concentrated at outer edge of the stain (see wiki "Coffee ring effect"). Both Asteroid belt and Kuiper belt (or part of Kuiper belt, see section III) can also be explained as the "ring stain", and one uses ice/rock mixture fragment as the "dye molecules", another one uses methane/ice mixture fragment as the "dye molecules". Or, we can say that the Kuiper belt is the "ring stain" of the current solar wind, and the Asteroid belt is the "ring stain" of an ancient fast expansion phase of the ice-evap-line.

Another explanation is, just like that geologists have told us that those large boulders in the New York central park was actually carried over by the glacial movement from hundreds kilometers away and then dumped here around 20000 to 12000 years ago (I learned this by watching a PBS public TV program, but can't find it now), or, we can say that the New York central park is the dumpsite for those glacial transported boulders, we can say that {1,8//6}o orbit shell (where the Asteroid belt sits now) was the dumpsite of the (slow speed) out-flying ice-rock mixture fragments driven by the fast expansion of the ice-evap-line, and {2,1//6}o orbit shell (where the Kuiper belt sits now) is the dumpsite of the out-flying methane/ice mixture fragments (driven by the expansion of methane-evap-line, or the solar wind stop line).

II. Using r^2*|R(n,*l*)|^2 *|Y(*l*,m)|^2 probability to build a belt at {1,8} = {0,48} orbit shows that Asteroid belt is in |48,47,47> QM state

One purpose of this paper is to pave the road for the next paper SunQM-3s11 to build a r^2 * |R(n,*l*)|^2 * |Y(*l*,m)|^2 3D probability density map for the whole Solar system. There, {0,1//6} is set to be n=1 for the primary (or master) r^2 * |R(n,*l*)|^2 * |Y(*l*,m)|^2 for the whole Solar system. So in current paper, we try to re-write a {N,n//6} as {0,n*6^N//6} whenever it is possible.

Now let's start to build the r^2 * |R(n,*l*)|^2 * |Y(*l*,m)|^2 for Asteroid belt. As we defined before |nLL> means |nlm> with *l* = n-1, and m = n-1 (see SunQM-3s1). By default, we should use the Sun's primary r^2 * |R(n,*l*)|^2 * |Y(*l*,m)|^2 where n=1 at Sun core (see paper SunQM-3s11 section-I), so Asteroid belt (formed by the QM's nLL effect at {1,8//6} = {0,48//6} orbit) is expected to be in |nLL> = |n,n-1,n-1> = |48,47,47> QM state. Let's first determine Asteroid belt's probability density curve in r-dimension to see whether it matches the experimental data. I am not able to obtain formulas of the radial wave function R(n,*l*) for n > 6. However, according to the R(n,*l*) formulas of R(6,5), R(5,4), R(4,3), R(3,2), and R(2,1), I am able to guess out that

$$R(n,l=n-1) \propto r_1^{(-3/2)} *(r/r_1)^{(n-1)} * \exp(-r/r_1/n) \qquad \text{eq-1}$$

Or, the r-dimension's probability is proportional to

$$r^2 *|R(n,l=n-1)|^2 \propto r^2 * |r_1^{(-3/2)} *(r/r_1)^{(n-1)} * \exp(-r/r_1/n)|^2 = r^2 * r_1^{(-3)} *(r/r_1)^{[2*(n-1)]} * \exp(-2*r/r_1/n) = r_1^{(-1)} *(r/r_1)^{(2*n)} * \exp(-2*r/r_1/n) \qquad \text{eq-2}$$

We know that at $r = r_n$, eq-2 produces a maximum value:

$$r_n^2 *|R(n,l=n-1)|^2 \propto r_1^{(-1)} *(r_n / r_1)^{(2*n)} * \exp(-2*r_n /r_1/n) \qquad \text{eq-3}$$

Notice that eq-3 is a constant value to r. Because during calculation, eq-2 produces some super large (or super small) values that chocks Excel's calculation, so we better to normalize eq-2 by its maximum value in eq-3,

$$r^2 *|R(n,l=n-1)|^2 \propto r1^{(-1)} *(r/r_1)^{(2*n)} * \exp(-2r/r_1/n) / [r_1^{(-1)} *(r_n / r_1)^{(2*n)} * \exp(-2*r_n /r_1/n)] \qquad \text{eq-4}$$

After simplification by using $r_n = r_1 * n^2$, we have the final normalized r-dimension probability function as

$$r^2 *|R(n,l=n-1)|^2 \propto [r/r_n * \exp(1 - r/r_n)]^{(2*n)} \quad \text{eq-5}$$

If we plot eq-5, we can see that it is an exponential rise curve $[r/r_n]^{(2*n)}$ times an exponential decline curve $[\exp(1 - r/r_n)]^{(2*n)}$, with the maximum always at r_n, and the higher the n, the narrower the peak.

Using eq-5 with n= 48, the normalized

$$r^2 *|R(48,47)|^2 \propto [r/4.01E+11 * \exp(1 - r/4.01E+11)]^{(2*48)} \quad \text{eq-6}$$

where $r_{n=48}$ = 4.01E+11 m (see SunQM-1s1 table 5). Table 1 (and Figure 1a) shows that eq-6 gives maximum probability at r_n=4.01E+11 m, or 2.69 AU, and the probability peak with 0.1 cut-off at 1.95 AU to 3.32 AU (or 2.7 ± 0.6 AU). The experimental data in Figure 1b shows that the core Asteroid belt's mass (in red) distributed from ~ 2.1 AU to ~ 3.3 AU, and it correlates exactly to Table 1's probability peak at ~ 10% cut-off (see the yellow and green marked cells in Table 1).

For a |nLL> = |48,47,47> QM state, let's check whether Asteroid belt's mass in θ-dimension distribution matches $|Y(l=47,m=47)|^2$ or not. For |n,*l*=n-1,m=n-1>, we know that (see John S. Townsed, A Modern Approach to Quantum Mechanics, 2nd ed., 2012, pp334, eq-9.146)

$$Y(l=n-1,m=n-1) \propto \exp[i*(n-1)*\varphi] * [\sin(\theta)]^{(n-1)} \quad \text{eq-7a}$$

or

$$Y(l,m) = \Theta(\theta) * \Phi(\varphi) \quad \text{eq-7b}$$

or

$$|\Theta(\theta)|^2 \propto [\sin(\theta)]^{[2*(n-1)]} \quad \text{eq-8}$$

Now let's set the probability peak cut-off at 0.01 for θ-dimension, and determine the delta θ range for it:

$$|\Theta(\theta)|^2 \propto [\sin(\theta)]^{[2*(n-1)]} = [\sin(\theta)]^{[2*(48-1)]} = [\sin(\theta)]^{94} = 0.01 \quad \text{eq-9}$$

Notice that in rθφ coordinates, $\theta = \pi/2 + \theta'$, so we have $\sin(\pi/2 + \theta') = \cos(\theta') = 0.01^{(1/94)}$, or $\theta' = \arccos[0.01^{(1/94)}]$ = 0.3105 arc = 17.8 degree. The experimental data in Figure 1b shows that Asteroid belt core mass' (in red) inclination distribution is within ~ 18 degree. Again it is perfectly matched. Notice that the minor blue colored mass which has inclination at around 20 to 25 degree belongs to |48,47,m> QM states with m < n-1=47. In this way we have confirmed that > 90% of mass in Asteroid belt is perfectly in |48,47,47> QM state.

Furthermore, we can use a integration formula to describe Asteroid belt in |48,47,47> QM state as

$$\text{Mass}(r, \theta, \varphi) = 2.94E+21 \text{ kg} = \iiint r^2 *|R(48,47)|^2 * |Y(47,47)|^2 * W *D *\sin(\theta)\ dr\, d\theta\, d\varphi, [r=0, 10*1.49E+11 \text{ m}; \theta=0, \pi; \varphi=0, 2\pi] \quad \text{eq-10}$$

where the radial integration from 0 meters, to 10 AU = 10* 1.49E+11 meters, the total mass of Asteroid belt is 2.94E+21 kg (see wiki "Asteroid belt"), D is the mass density in Asteroid belt, and W is the factor to make the whole integration equals to 2.94E+21 kg.

In r-dimension, if using |n=49,l=n-1,m=n-1>, then its r = 2.75 ± 0.6 AU (at 10% probability cut-off). This is not much different from |48,47,47> 's r=2.69 ± 0.6 AU. So at ~ 50% (or any adequate %) probability cut-off, Asteroid belt's |48,47,47> QM state probably can also described by a linear combination of n= … 46, 47, 48, 49, 50, … QM states. Obviously, in general, a single n QM description is more adequate than a combination of many n(s) QM description.

Similarly in θ-dimension, even at a single n=48 QM state, a |n=48,*l*=n-1=47,m=n-2=46> QM state has θ' = 8.4° ± ~10° (from 0.5° to 22.7° at 1% probability cut-off, or from 1.7° to 18.4° at 10% probability cut-off). This is also not much different from the |n=48,l=47,m=n-1=47> QM state's θ' = 0° ± 17.8° at 1% probability cut-off, or θ' = 0° ± 12.6° at 10% probability cut-off. So in θ-dimension, at ~ 50% (or any adequate %) probability cut-off, Asteroid belt's |48,47,47> QM state probably can also be described by a linear combination of |48,47,m> QM states with m= … n-2, n-1, n, … = … 46, 47, 48, … . Again, in general, a single m QM description is more adequate than a combination of many m(s) QM description. So we choose |48,47,47> rather than a combination of |n=..47,48,49..,*l*,m=..n-2,n-1,n..> to describe Asteroid belt. Note: For |n,n-1,n-2> QM state's |Θ(θ)|^2 calculation, according to wiki "Table of spherical harmonics", I guessed out that

$$|\Theta(\theta)|^2 \propto [\sin(\theta)]^{2(n-2)}*[\cos(\theta)]^2 \qquad \text{eq-8b}$$

A manual searching was used to estimate the θ value at different probability % cut-off (data not shown here).

Table 1. Asteroid belt's r^2 *|R(48,47)|^2 probability curve calculation, with maximum at r/r_1 = n^2 =48^2, or 4.01E+11 m, or 2.69 AU.

n=	48		
r_1= (a=)	1.74E+08	meter	
r/r_1=	r^2 *|R(48,47)|^2	r= (m)	r= (AU)
4.8	1.57E-216	8.35E+08	0.01
1665.6	1.05E-02	2.90E+11	1.95
1728	2.67E-02	3.01E+11	2.02
1838.4	1.03E-01	3.20E+11	2.15
1920	2.22E-01	3.34E+11	2.24
2016	4.39E-01	3.51E+11	2.35
2112	7.01E-01	3.67E+11	2.47
2208	9.17E-01	3.84E+11	2.58
2304	1.00E+00	4.01E+11	2.69
2400	9.23E-01	4.18E+11	2.80
2496	7.31E-01	4.34E+11	2.91
2592	5.02E-01	4.51E+11	3.03
2688	3.02E-01	4.68E+11	3.14
2784	1.61E-01	4.84E+11	3.25
2846.4	1.00E-01	4.95E+11	3.32
2976	3.26E-02	5.18E+11	3.48
3072	1.26E-02	5.35E+11	3.59
3264	1.43E-03	5.68E+11	3.81
3840	3.23E-07	6.68E+11	4.48
4608	1.65E-13	8.02E+11	5.38

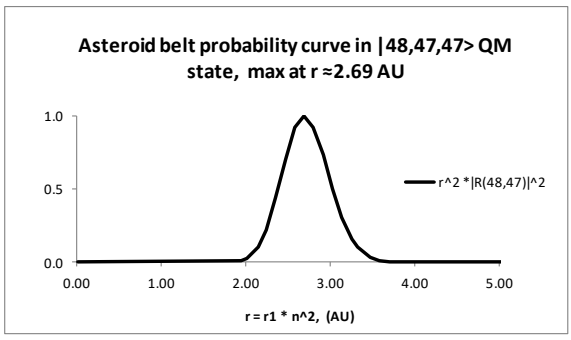

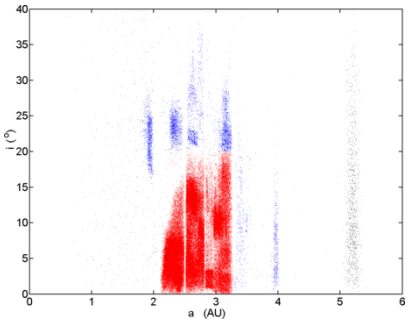

Figure 1a (left). Asteroid belt's r^2 *|R(48,47)|^2 probability curve, with maximum at 2.69 AU.
Figure 1b. The asteroid belt showing the orbital inclinations versus distances from the Sun, with asteroids in the core region of the asteroid belt in red and other asteroids in blue. Copied from [15]. Author: Piotr Deuar. Copy right: CC BY-SA 3.0.

III. Using r^2 *|R(n,*l*)|^2 *|Y(*l*,m)|^2 probability function to build a belt at {2,6} orbit shows that the "cold" classical Kuiper belt is in |192,191,191> QM state

According to wiki "Kuiper belt", Kuiper belt "*is a circumstellar disc in the outer Solar System, extending from the orbit of Neptune (at 30 AU) to approximately 50 AU from the Sun*". In {N,n//6} QM, for the uncompressed orbit shell space calculation, {2,5//6} = {0,5*6^2//6} = {0,180//6}, {2,6//6} = {0,6^3//6} = {0,216//6}, and {2,7//6} = {0,7*6^2//6} = {0,252//6}. Because N=2 super-shell is compressed with pFactor = 5.33 (not equals to 6), so the real total n for {2,5//6} = {0,5*6*5.33//6} ≈ {0,160//6}, {2,6//6} = {0,6*6*5.33//6} ≈ {0,192//6}, and {2,7//6} = {0,7*6*5.33//6} ≈ {0,224//6}. According to Solar {N,n//6} QM structure model (see Table 3 of SunQM-1), Neptune's {2,5//6}o orbit shell covers from 30 AU to 43 AU from the Sun, and {2,6//6}o orbit space ends at {2,7//6} with $r_n = r_1*n^2$ =1.74E+8 * 224^2 = 8.72E+12 m = 58.5 AU, so it covers from ~ 43 AU to ~ 58.5 AU from the Sun. From wiki "*Distribution of cubewanos (or The Classical Kuiper belt object, blue), Resonant trans-Neptunian objects (red), Sednoids (yellow) and scattered objects (grey)*" [16], also copied as Figure 2a here, most objects in the {2,5//6}o orbit shell are belong to the Scattered disc (see wiki "Scattered disc"), and almost all Kuiper belt objects are located in the r ≈ 40 AU to 50 AU region.

This data tells us a lot of information:

1) It confirms (with good accuracy) the existence of an orbit shell that starts from 43 AU (that was predicted from Solar {N,n//6} QM structure model), and it belongs to Kuiper belt's {2,6//6}o orbit shell.

2) Let's use {2,6//6}o orbit with n=6 for analysis. Let's first review the knowledge we have learned from paper SunQM-3s4 section I-b "*Using n=4 radial probability curve to explain how Saturn ring collapse as the ring mass decreasing*". For n=4, r^2 * |R(n,*l*)|^2 has maximum value at r_n/r_1= 16 for |43m>, r_n/r_1≈ 21 for |42m>, r_n/r_1≈ 24 for |41m>, and r_n/r_1≈ 25 for |400> QM states. Then, as the ring mass decreasing, the ring width (Δr) will decrease within the same n=4 shell space. So while the inner edge of ring keeps at r_n/r_1=16, the outer edge of the ring will quantum collapse from r_n/r_1≈ 25 of |400> state, to r_n/r_1≈ 24 of |411> state, then to r_n/r_1≈ 21 of |422> state, finally to r_n/r_1≈ 16 of |433> state. For n=5, Table 2 in paper SunQM-3 tells us that r^2 * |R(n,*l*)|^2 has maximum values at r_n/r_1= 25 for|54m>, r_n/r_1≈ 33 for |53m>, r_n/r_1≈ 36 for |52m>, r_n/r_1≈ 38 for |51m>, and r_n/r_1≈ 39 for |50m>. Now for n=6, although I can't find the R(n,*l*) function for *l* = 0, 1, 2, 3, 4, I can guess that the r^2 * |R(n,*l*)|^2 has maximum value at r_n/r_1= 36 for |65m>, $r_n/r_1 \geq$ 45 for |64m>, $r_n/r_1 \geq$ 49 for |63m>, r_n/r_1≈ 52 for |62m> QM states, etc. Remember this is for the non-compressed $r_n/r_1 = n^2$. For N=2 super-shell compressed r_n/r_1, above calculation needs to multiply (5.33/6)^2. For {2,1//6}, r_1=2.25E+11 m, so the r^2 * |R(n,*l*)|^2 has maximum value at r_n= 36 *(5.33/6)^2 *2.25E+11 = 43 AU for |65m>, or at $r_n \geq$ 45 *(5.33/6)^2 *2.25E+11 ≈ 54 AU for |64m>, or at $r_n \geq$ 49 *(5.33/6)^2 *2.25E+11 ≈ 58 AU for |63m>, etc. So the fact that almost all Kuiper belt objects are located in the r = 40 AU to 50 AU range implies that most Kuiper belt objects are in the lowest (r-dimensional) energy |65m> QM states.

3) Let's use {2,6//6}o orbit space covering from {0,192//6}={2,6//6} to {0,224//6}={2,7//6}, or from n=192, to n=224 for analysis. Based on the fact that almost all Kuiper belt objects are located in the r = 40 AU to 50 AU range, we need to figure out are Kuiper belt objects in the n=192 state along, or in a combination of many n(s) states from 192 to 224? The best way to do this is to use eq-5 for n=192, and to see whether the probability peak fits to 40 AU to 50 AU range. So, using eq-5, the normalized

$$r^2 *|R(192,191)|^2 \propto [r / 6.40E+12 * \exp(1 - r / 6.40E+12)]^{(2*192)} \quad \text{eq-11}$$

where r_n = 6.40E+12 m (see SunQM-1 table 3). Eq-11 was calculated in Table 2 and plotted in Figure 2b. The result shows that Kuiper belt's r^2 *|R(192,191)|^2 probability curve has the maximum at r = 43 AU. It has the ~10% probability (or 90% down) range from ~38.5 AU to ~ 47.8 AU, or about (43 ± 5) AU, practically the same as Figure 2a's result.

According to Asteroid belt's result, we strongly believe that Kuiper belt is in |192,191,191> QM state. If this is correct, then we can predict Kuiper belt's mass distribution in the θ-dimension. Similar as that in eq-9, let's set the probability peak cut-off at 0.01 for θ-dimension, and determine the delta θ range for it:

$|\Theta(\theta)|^2 \propto [\sin(\theta)]^{[2*(n-1)]} = [\sin(\theta)]^{[2*(192-1)]} = [\sin(\theta)]^{382} = 0.01$ eq-12

Using $\theta = \pi/2 + \theta'$, we have $\sin(\pi/2 + \theta') = \cos(\theta') = 0.01^{(1/382)}$, $\theta' = \arccos[0.01^{(1/382)}] = 0.155$ arc = 8.9 degree. The calculation predicts that > 90% of mass in Kuiper belt has orbit inclination within 8.9 degree. If using probability cut off = 0.1, then $\theta' = \arccos[0.1^{(1/382)}] = 0.110$ arc = 6.3 degree. In Figure 2a, the blue objects are called "the classical Kuiper belt object", or "cubewanos". Wiki "Classical Kuiper belt object" mentioned "*The majority of classical objects, the so-called cold population, have low inclinations (< 5°) and near-circular orbits, lying between 42 and 47 AU. A smaller population (the hot population) is characterized by highly inclined, more eccentric orbits*". Let's name the "cold" classical KBO population as "**cold-KBO**", and the "hot" classical KBO population as "**hot-KBO**". Our result shows that the cold-KBO can be perfectly described by the |192,191,191> QM state, and the hot-KBO can be described |192,191,m> QM states where m is a combination of integers < 191.

Similar as that for Asteroid belt, if we choose the probability cut-off at ~ 50% (or any adequate %) in r- (or θ-) dimension, then the cold-KBO at | 192, 191, 191> can also be described by a combination of |n,l,m> QM states with n(s) = … 190, 191, 192, 193, …, and/or m(s) = … (n-2), (n-1), n, … . Again, in general, a single n (or a single m) QM description is more adequate than a combination of many n(s) (or many m(s)) QM description. So we choose |192,191,191> rather than a combination of |n=..191,192,193..,l,m=..n-2,n-1,n..> to describe the cold-KBO.

Also we can use a integration formula to describe cold-KBO in |192,191,191> QM state as

$$\text{Mass}(r, \theta, \varphi) = \iiint r^2 * |R(192,191)|^2 * |Y(191,191)|^2 * W * \sin(\theta)\ dr\ d\theta\ d\varphi,\ [r=0, 100*1.49E+11\ m;\ \theta=0, \pi;\ \varphi=0, 2\pi] \quad \text{eq-13}$$

where the radial integration from 0 m, to 100 AU = 100* 1.49E+11 m, and W is the factor to make the whole integration equals to the cold-KBO's total mass.

The fact that both Asteroid belt and cold-KBO can be perfectly and completely described by a single n valued |n*l*m> QM state suggesting that n=1 at {0,1//6} is the good r_1 for the master r^2 * |R(n,*l*)|^2 * |Y(*l*,m)|^2 for the whole Solar system.

Table 2. Cold-KBO's r^2 *|R(192,191)|^2 probability curve calculation, with maximum at r = 43 AU.

n=	192		
r_1= (a=)	1.74E+08	meter	
r/r_1= (n^2)	r^2 *|R(192,191)|^2	r= (m)	r= (AU)
192	0.00E+00	3.3E+10	0.2
31104	5.83E-03	5.4E+12	36.3
32256	4.08E-02	5.6E+12	37.7
32928	1.01E-01	5.7E+12	38.5
33792	2.56E-01	5.9E+12	39.5
34560	4.75E-01	6.0E+12	40.4
34944	6.02E-01	6.1E+12	40.8
35328	7.28E-01	6.1E+12	41.3
35712	8.41E-01	6.2E+12	41.7
36096	9.30E-01	6.3E+12	42.2
36480	9.85E-01	6.3E+12	42.6
36864	1.00E+00	6.4E+12	43.0
37248	9.73E-01	6.5E+12	43.5
37632	9.09E-01	6.5E+12	43.9
38016	8.16E-01	6.6E+12	44.4
38400	7.04E-01	6.7E+12	44.8
38784	5.85E-01	6.7E+12	45.3
39552	3.61E-01	6.9E+12	46.2
40320	1.93E-01	7.0E+12	47.1
40972.8	1.01E-01	7.1E+12	47.8
41856	3.63E-02	7.3E+12	48.9
43776	2.18E-03	7.6E+12	51.1
73728	3.61E-52	1.3E+13	86.1

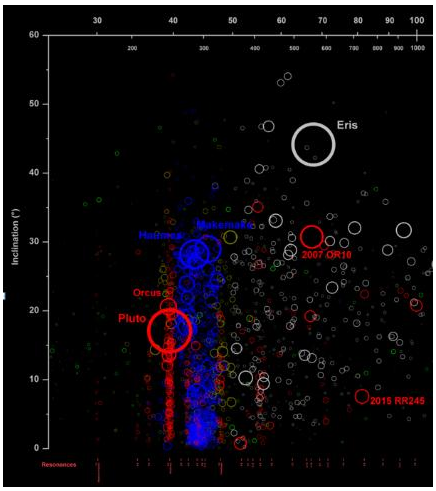

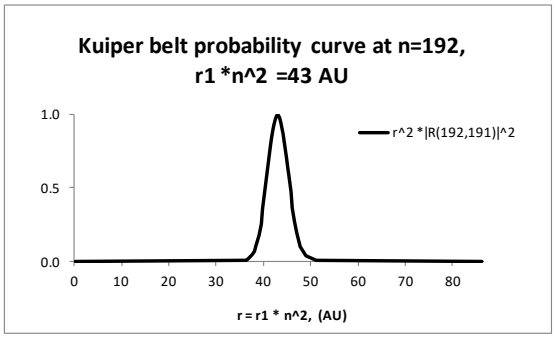

Figure 2a (left). Distribution of cubewanos (or The Classical Kuiper belt object, blue), Resonant trans-Neptunian objects (red), Sednoids (yellow) and scattered objects (grey). Copied from [16]. Author: Renerpho. Copy right: CC BY-SA 4.0.
Figure 2b (right). Demonstration of Kuiper belt's r^2 *|R(192,191)|^2 probability curve at n=192, with maximum at r/r_1 = n^2 =36864, or r = 43,3 AU, using r = r_1 * n^2 as x-axis.

IV. New concept: Eigen quantum number n' is the maximum n' that can describe one orbit space's > 90% mass in a single |nLL> = |n',n'-1,n'-1> QM state

Let's use Kuiper as the example in r-dimension and use Kuiper belt's cold-KBO as the example in θ-dimension. We know Kuiper belt is at {2,6//6}o orbit space, which has position of {3,1//6}. For easy analysis, let's (momentarily) ignore the pFactor = 5.33 at N=2 super-shell, and assume it is still =6. Based on the {N,n//6} QM, we know that a orbit at {3,1//6} has n=1, and r_1 at r of {3,1//6} with r_1= 1.74E+8 *(6^2)^3 = 8.12E+12 m. Meanwhile, it can also have n=6, and r_1 at r of {2,1//6} with r_1= 1.74E+8 *(6^2)^2 = 2.26E+11 m, or has n=6^2=36, and r_1 at r of {1,1//6} with r_1= 1.74E+8 *(6^2) = 6.26E+9 m, or has n=6^3=216, and r_1 at r of {0,1//6} with r_1= 1.74E+8 m. No matter what n and r_1 we use, a {3,1//6} positioned belt in the (N=2 super-shell non-compressed) Solar {N,n//6} QM structure will always have r_n = r_1 *n^2 = 54.5 AU. Table 3 shows the calculations for a belt at 54.5 AU (with 90% mass containing within 55 ± 5.5 AU) to be described by r^2 * |R(n,*l*)|^2 probability curve at n=6^3, 6^2, 6, 1, 1/6. All r^2 *|R(n,n-1)|^2 functions are constructed according to eq-5 (with r_n = r_1 *n^2). The resulted probability curves are plotted in Figure 3. So Table 3 and Figure 3 shows that a {3,1//6} positioned belt can be described by a n=1 with r_1 at {3,1//6}, or r^2 * |R(1,0)|^2 curve, with ~10% probability (or 90% down) range from ~7.6 AU to >> 114 AU. It also shows that when the same belt is described by n=6 with r_1 at {2,1//6}, or a r^2 * |R(6,5)|^2 curve, it will have ~10% probability range from ~27 AU to ~95 AU, or when described by a n=6^2=36 with r_1 at {1,1//6}, or a r^2 * |R(36,35)|^2 curve, it will have ~10% probability range from ~42 AU to ~69 AU, or when described by a n=6^3=216 with r_1 at {0,1//6}, or a r^2 * |R(216,215)|^2 curve, it will have ~10% probability range from ~49 AU to ~60 AU. We see that the higher the high-frequency n' goes, the narrower the r-dimension range it covers, and of course, the lower the n' goes, the wider the r-dimension range it covers. So at n=6^3=216 with r^2 * |R(216,215)|^2 curve, with ~10% probability covers range (54.5 ± 5.5) AU, very close to Kuiper belt's (43 ± 5) AU. In the real situation, due to the pFactor =5.33 at N=2 super-shell, Kuiper belt at orbit at {3,1//6} has n=1 with r_1 at r of {3,1//6}. or n=5.33 with r_1 at r of {2,1//6}, or n =5.33 *6 =32 with r_1 at r of {1,1//6}, or n =5.33 *6^2 =192 with r_1 at r of {0,1//6} and with r_n = r_1 * n^2 = 1.74E+8 * 192^2 /1.49E+11 = 43 AU. The purpose of this calculation is to show that only at n'= 192, the r^2 *|R(192,191)|^2 curve have the peak range = (43 ± 5) AU, just right for Kuiper belt's mass distribution in r-dimension. This means that n'= n*q^w = 1*5.33*6^2 = 192, not only describe Kuiper belt is at {3,1//6} orbit (using n*q^w = 1*5.33*6^2 information), but also has the mass distribution information in r-dimension with peak at 43 AU, and the width of peak at ±5 AU. Here we define this n' as the "Eigen quantum number n' ", because it gives the correct width (besides the correct orbit position) of the probability peak. So

n'=192 is the Eigen n' for Kuiper belt. If we use n'=1*5.33*6^1 =32, then according the Table 3b, the peak range from =41.9*(5.33/6)^2 =33 AU to = 69.4*(5.33/6)^2 = 54.8 AU, or 43 ±11 AU. So it is too broad for Kuiper belt's 43± 5 AU.

Figure 3 shows that among n'=1*6^(-1) = 1/6, n'=1, n'=5.33, n'=1*5.33*6^1 =32, and n'=1*5.33*6^2 =192, the higher the n' value, the narrower the probability peak. So, the Eigen quantum number n' is the maximum n' that can describe one orbit space's > 90% mass in a single |nLL> = |n',n'-1,n'-1> QM state. Then, what about if we choose the even higher n', e.g., n'=1*6^5 =7776 (as shown in Table 3f)? The answer is then we need to use a combination of many n'(s), e.g., n'= … 7774, 7775, 7776, 7777, 7778, … to cover Kuiper belt's mass r-distribution range 43 ± 5 AU. Furthermore, for these n'= … 7774, 7775, 7776, 7777, 7778, …, they are no longer in nLL QM states.

So if a belt (or any object) can be perfectly described by a |n',n'-1,n'-1>, we name this is a "Eigen description", and this n' is the "Eigen quantum number", and the |n',n'-1,n'-1> is "Eigen QM state", and the r^2 *|R(n',n'1)|^2 *Y(n'-1,n'-1)|^2 is the "Eigen probability curve". Eigen quantum number n' usually is one of the high-frequency n'(s). For a belt, Eigen n' gives the information of not only the orbit r, but also the belt's size (in r- and θ-dimension). For a planet, Eigen n' gives the information of not only the orbit r, but also the planet's size (in rθφ 3D-dimensions). So in the Eigen QM state, n', *l* =L =n'-1, m =L =n'-1 are always single valued as |n',*l*=n'-1,m=n'-1>. Any sub-Eigen n' description for this Eigen QM state will be a low resolution and more broad description. Any above Eigen n' description for this Eigen QM state will be a high resolution but needs many linearly combined QM states.

Some examples of "Eigen probability curve" in r-dimension: 1) In Figure 1a, |48,47,47> with r_1 at {0,1//6} is the "Eigen QM state" for Asteroid belt; 2) In Figure 2b, |192,191,191> with r_1 at {0,1//6} is the "Eigen QM state" for the cold-KBO. 3) Broadly speaking, Figure 4a presented QM states can also be called Eigen QM states (in r-dimension only, see section VI): the whole N=1 super shell space's mass is in the Eigen $n'_r = 4$ QM state, with r^2*|R(n=4,*l*=3)|^2 probability, and with r_1 at {1,1//6}; the whole N=2 super shell space's mass is in the Eigen $n'_r = 2$ QM state, with r^2*|R(n=2,*l*=1)|^2 probability, and with r_1 at {2,1//6}; the whole {N=1..4,n} region of the Solar system is in the Eigen n'_r =4/6^2 QM state, with r^2*|R(n=4/6^2,*l*=n-1)|^2 probability, and with r_1 at {3,1//6}.

Not only r-dimension has the "Eigen probability curve", both θ-dimension and φ-dimension also have the "Eigen probability curve". Some examples of "Eigen probability curve" in θ- or φ-dimension are: 1) Asteroid belt's |48,47,47> QM state produces the Eigen probability curve in θ- dimension with n'_θ =48 (see section II); 2) The cold-KBO's |192,191,191> QM state is expected to produce the Eigen probability curve in θ- dimension with n'_θ =192 (see section III); 3) Earth surface r's Eigen n'= 5*6^11=1813985280 in all r-, θ-, and φ-dimensions (see SunQM-3s11 Table 1). This n' confines a probability density peak (at 0.01 cut-off) within the space of 2* 7.89E+6 m in rθφ 3D-dimensions, and at $r_{n'}$ = 1.57E+11 m. The same n' confines a probability density peak (at 0.05 cut-off) within the space of 2* 6.38E+6 m in rθφ 3D-dimensions, and at $r_{n'}$ = 1.57E+11 m. Both fit to Earth's size and orbit r accurately.

In general, each planet size's Eigen n'(s) are the same in rθφ 3D-dimensions, or $n'_r = n'_\theta = n'_\varphi$ (see SunQM-3s11 Table 1). Each belt's Eigen n'(s) are expected to be the same in r and θ 2D-dimensions, or $n'_r = n'_\theta$ (see results of Asteroid belt and the cold-KBO) although in some cases $n'_r \neq n'_\theta$. For example, the whole Kuiper belt's $n'_r < n'_\theta$, and Saturn B ring's $n'_r << n'_\theta$, with an extremely high n'_θ value (= 4*3^25 =3.39E+12, see SunQM-3s4 section-Id).

In SunQM-3s11 we named a "primary form" {N,n//q} where N ≡ 0, and it is written as {0,n*q^N//q} or |n*q^N,*l*,m>. It should be pointed out that the "Eigen QM state" has different meaning than the "primary form" |n*q^N,*l*,m>. Although in some special cases they are the equivalent (e.g., for Kuiper belt, the primary form |6*5.33*6^1,*l*,m> is similar as the Eigen QM state |192,191,191>), in general, they are unrelated and have different forms.

One interesting point from the Table 3 calculation is that at n=1/6, *l* = n-1 = -5/6, or *l* become a negative value. However, the eq-5 is still valid for the probability curve calculation! It seems that in the {N,n//q} QM, in the Schrodinger equation's wave function R(n,*l*) Y(*l*,m), *l* can be negative when n < 1. Does this negative *l* has a real physics meaning, or it is only a mathematical processing? So far I do not know.

Figure 3 shows us one new concept in the {N,n//q} QM physics (and probably one of the most important concepts in physics): in r-dimension, while a base frequency n (with numbers from 1 to 10)'s {N,n//q} QM is the best description for the QM physics at r position, a sub-base-frequency n (< 1)'s {N,n//q} QM is a top-down description method which provides a low resolution of the whole picture for the large Δr range (with r_1 much larger than the r we are interesting), and a high-frequency multiplier n' provides a high resolution of a picture within a short Δr range (with r_1 much smaller than the r we are interesting).

It may also contain an uncertainty principle kind relationship: the smaller the r_1, the larger n it can describe, or r_1 * n^2 = r_n where r_n is a fixed value. Remember H*n = constant (in SunQM-2 section I-g)? It is exactly the same. This is because H = h/m' = 2π *sqrt(GMr_1), so H*n = 2π *sqrt(GMr_1) *n = 2π *sqrt(GMr_n) = constant. For a specific n orbit, r_n is a constant. So in a point central force (Gravity or Electromagnetic, or other forces) formed {N,n//q} QM structure, H*n = constant may also be one kind of uncertainty principle.

It is like that a small piece of hologram still give the whole picture information (although with low resolution), the large piece give the more complete information, or like a SVD matrix converted picture for digital transportation, a smaller file still contains the whole picture, although with low resolution. So both Fourier transformation and matrix conversion are good tools for this kind of analysis. In section VI, we will use this property to explain the mass density r-distribution (and evolution) in Solar system's {N=1..4,n} region by using the r^2 * |R(n,*l*)|^2 * |Y(*l*,m)|^2 curve.

In the next paper (SunQM-3s11), we will use Eigen n' calculation to build a time-dependent 3D probability density map that directly matches our current Solar system.

Table 3 (a, b, c, d, e, f, from left to right). Calculations to demonstrate that a belt at 54.5 AU (with 90% mass within range of r = 55 ± 5.5 AU), can be described by r^2 * |R(n,*l*)|^2 curve at n=1/6, 1, 6, 6^2, 6^3, 6^5, etc.

r1 at {0,1//6}, max at {3,1//6} or n=6^3			
max.prob. n=		216	
r_1 at		{0,1//6}	
r_1=		1.74E+08	m
r/r_1=	r= r/r1*r1	r^2*|R(216,215)|^2	r, AU
27216	4.74E+12	1.12E-23	31.8
29376	5.11E+12	4.92E-18	34.3
31536	5.49E+12	2.08E-13	36.8
33696	5.86E+12	1.15E-09	39.3
35856	6.24E+12	1.08E-06	41.9
38016	6.61E+12	2.09E-04	44.4
40176	6.99E+12	1.01E-02	46.9
42120	7.33E+12	1.13E-01	49.2
44496	7.74E+12	6.20E-01	52.0
46656	8.12E+12	1.00E+00	54.5
48816	8.49E+12	6.38E-01	57.0
51624	8.98E+12	1.01E-01	60.3
53784	9.36E+12	1.02E-02	62.8
55296	9.62E+12	1.36E-03	64.6
57456	1.00E+13	4.32E-05	67.1
59616	1.04E+13	7.47E-07	69.6
61776	1.07E+13	7.33E-09	72.1
63936	1.11E+13	4.24E-11	74.7
66096	1.15E+13	1.49E-13	77.2
68256	1.19E+13	3.33E-16	79.7

r1 at {1,1//6}, max at {3,1//6} or n=6^2			
max.prob. n=		36	
r_1 at		{1,1//6}	
r_1=		6.26E+09	m
r/r_1=	r= r/r1*r1	r^2*|R(36,35)|^2	r, AU
648	4.06E+12	9.13E-07	27.2
720	4.51E+12	3.29E-05	30.3
792	4.96E+12	5.77E-04	33.3
864	5.41E+12	5.55E-03	36.3
936	5.86E+12	3.24E-02	39.3
996	6.24E+12	1.01E-01	41.9
1080	6.77E+12	3.24E-01	45.4
1152	7.22E+12	6.19E-01	48.4
1224	7.67E+12	8.91E-01	51.5
1296	8.12E+12	1.00E+00	54.5
1368	8.57E+12	8.98E-01	57.5
1440	9.02E+12	6.61E-01	60.5
1512	9.47E+12	4.06E-01	63.6
1584	9.92E+12	2.12E-01	66.6
1650	1.03E+13	1.02E-01	69.4
1728	1.08E+13	3.74E-02	72.6
1800	1.13E+13	1.29E-02	75.7
1872	1.17E+13	3.99E-03	78.7
1944	1.22E+13	1.11E-03	81.7
2016	1.26E+13	2.78E-04	84.8

r1 at {2,1//6}, max at {3,1//6} or n=6			
max.prob. n=		6	
r_1 at		{2,1//6}	
r_1=		2.26E+11	m
r/r_1=	r= r/r1*r1	r^2*|R(6,5)|^2	r, AU
9	2.03E+12	4.83E-04	13.6
12	2.71E+12	5.61E-03	18.2
15	3.38E+12	3.00E-02	22.7
18.1	4.08E+12	1.02E-01	27.4
21	4.74E+12	2.30E-01	31.8
24	5.41E+12	4.21E-01	36.3
27	6.09E+12	6.36E-01	40.9
30	6.77E+12	8.29E-01	45.4
33	7.44E+12	9.57E-01	49.9
36	8.12E+12	1.00E+00	54.5
39	8.79E+12	9.61E-01	59.0
42	9.47E+12	8.61E-01	63.6
45	1.01E+13	7.24E-01	68.1
48	1.08E+13	5.78E-01	72.6
51	1.15E+13	4.40E-01	77.2
54	1.22E+13	3.22E-01	81.7
57	1.29E+13	2.26E-01	86.3
63	1.42E+13	1.02E-01	95.3
66	1.49E+13	6.55E-02	99.9
76.8	1.73E+13	1.10E-02	116.2

r1 at {3,1//6}, max at {3,1//6} or n=1			
max.prob. n=		1	
r_1 at		{3,1//6}	
r_1=		8.12E+12	m
r/r_1=	r= r/r1*r1	r^2*|R(1,0)|^2	r, AU
0.1	8.12E+11	6.05E-02	5.4
0.14	1.14E+12	1.09E-01	7.6
0.3	2.44E+12	3.65E-01	16.3
0.4	3.25E+12	5.31E-01	21.8
0.5	4.06E+12	6.80E-01	27.2
0.6	4.87E+12	8.01E-01	32.7
0.7	5.68E+12	8.93E-01	38.1
0.8	6.49E+12	9.55E-01	43.6
0.9	7.31E+12	9.89E-01	49.0
1	8.12E+12	1.00E+00	54.5
1.1	8.93E+12	9.91E-01	59.9
1.2	9.74E+12	9.65E-01	65.4
1.3	1.06E+13	9.27E-01	70.8
1.4	1.14E+13	8.81E-01	76.3
1.5	1.22E+13	8.28E-01	81.7
1.6	1.30E+13	7.71E-01	87.2
1.7	1.38E+13	7.13E-01	92.6
1.8	1.46E+13	6.54E-01	98.1
1.9	1.54E+13	5.97E-01	103.5
2.1	1.70E+13	4.89E-01	114.4

r1 at {4,1//6}, max at {3,1//6} or n=1/6			
max.prob. n=		1/6	
r_1 at		{4,1//6}	
r_1=		2.92E+14	m
r/r_1=	r= r/r1*r1	r^2*|R(n=1/6,l=n-1)|^2	r, AU
1.67E-04	4.87E+10	2.53E-01	0.3
1.11E-03	3.25E+11	4.71E-01	2.2
4.44E-03	1.30E+12	7.18E-01	8.7
7.78E-03	2.27E+12	8.32E-01	15.3
1.11E-02	3.25E+12	9.00E-01	21.8
1.44E-02	4.22E+12	9.44E-01	28.3
1.78E-02	5.20E+12	9.72E-01	34.9
2.11E-02	6.17E+12	9.89E-01	41.4
2.44E-02	7.14E+12	9.97E-01	47.9
2.78E-02	8.12E+12	1.00E+00	54.5
3.11E-02	9.09E+12	9.98E-01	61.0
3.44E-02	1.01E+13	9.92E-01	67.6
3.78E-02	1.10E+13	9.83E-01	74.1
4.11E-02	1.20E+13	9.71E-01	80.6
4.44E-02	1.30E+13	9.58E-01	87.2
4.78E-02	1.40E+13	9.42E-01	93.7
5.11E-02	1.49E+13	9.26E-01	100.3
5.44E-02	1.59E+13	9.09E-01	106.8
5.78E-02	1.69E+13	8.91E-01	113.3
6.11E-02	1.79E+13	8.72E-01	119.9

r1 at {-2,1//6}, max at {3,1//6} or n=6^5			
max.prob. n=		7776	
r_1 at		{-2,1//6}	
r_1=		1.34E+05	m
r/r_1=	r= r/r1*r1	r^2*|R(6^5,6^5-1)|^2	r, AU
5.36E+07	7.19E+12	2.52E-48	48.3
5.43E+07	7.30E+12	7.60E-38	49.0
5.51E+07	7.40E+12	9.48E-29	49.7
5.59E+07	7.51E+12	5.35E-21	50.4
5.67E+07	7.61E+12	1.49E-14	51.1
5.75E+07	7.71E+12	2.22E-09	51.8
5.82E+07	7.82E+12	1.92E-05	52.5
5.90E+07	7.92E+12	1.04E-02	53.2
5.97E+07	8.01E+12	2.73E-01	53.8
6.05E+07	8.12E+12	1.00E+00	54.5
6.12E+07	8.22E+12	2.79E-01	55.2
6.19E+07	8.32E+12	1.04E-02	55.8
6.27E+07	8.42E+12	2.61E-05	56.5
6.35E+07	8.53E+12	6.01E-09	57.2
6.43E+07	8.63E+12	1.34E-13	57.9
6.51E+07	8.73E+12	3.08E-19	58.6
6.58E+07	8.84E+12	7.67E-26	59.3
6.66E+07	8.94E+12	2.18E-33	60.0
6.74E+07	9.05E+12	7.43E-42	60.7
6.82E+07	9.15E+12	3.19E-51	61.4

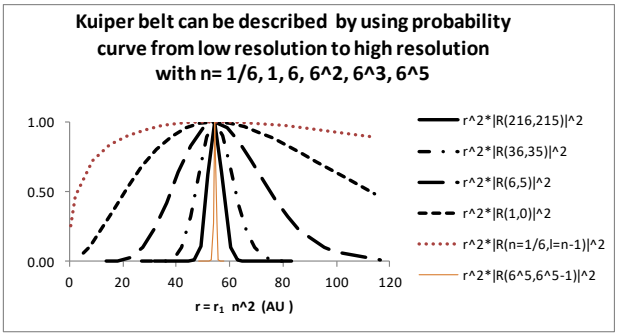

Figure 3. Demonstration of a belt at ~54.5 AU (with 90% mass within 55 ± 5.5 AU), can be described by r^2 * |R(n,*l*)|^2 curve at either n=1/6, 1, 6, 6^2, 6^3, 6^5, etc.

V. Predict Δr and Δθ' range for the undiscovered {3,n=2..5//6} belts by using r^2 * |R(n,*l*=n-1)|^2 curve

The four undiscovered {3,n=2..5//6} planets/belts are in {0,384//6}, {0,576//6}, {0,768//6}, {0,959//6} orbits in the Sun's primary {0,n*q^w//6} QM structure. If they do in the belt form, then just like Asteroid belt and the cold KBO, they are

expected to be in the Eigen |nLL> QM states of |384,383,383>, |576,575,575>, |768,767,767>, or |959,958,958> respectively. Using the same method in section II, we are able to predict that their r-dimension's mass distribution are in ranges of 173 ±13 AU, 390 ±25 AU, 693 ±38 AU, and 1081 ±53 AU, respectively. Also the (collection of most objects') orbits inclination distribution in θ-dimension for each belt is predicted to be within 6.3 degree, 5.1 degree, 4.4 degree, and 4.0 degree, respectively.

VI. Using r^2 *|R(n,*l*)|^2 * |Y(*l*,m)|^2 to explain the mass density r-distribution and its evolution in Solar system's {N=1..4,n} region

As mentioned in paper SunQM-1s1, after a pre-Sun ball quantum collapsed from {6,1} to the current {0,2}, the leftover mass density radial distribution in Solar system's {N=1..4,n} region (with < 1% mass occupancy) is described (approximately) by the equation

$$D(r) = 4.37E+28 / r^{3.279} \text{ (kg/m}^3\text{)} \qquad \text{eq-14}$$

This D(r) was assumed to be the original mass density r-distribution for Solar system (immediately after the pre-Sun collapse to {0,2}). Figure 2 of SunQM-3s2 showed a snapshot picture of some (disk-lyzing) disks when the pre-Sun's disk was forming (which was calculated purely from {N,n} QM). Also in paper SunQM-1s1, the abnormal high mass in Jupiter was explained as the result of capturing of icy-mass evaporated from inside the {2,1} QM structure after the ice-evap-line expanded and passed the {2,1}. With the success of using the Eigen probability curve r^2 * |R(n,*l*)|^2 * |Y(*l*,m)|^2 in describing the Asteroid belt and the cold-KBO, now we try to use the same method to describe the mass density r-distribution and its evolution in Solar system's {N=1..4,n} region.

Table 4 uses {N,n//6} QM model to calculate the current mass density r-distribution in Solar system's {N=1..4,n} region. The result shows that the maximum mass density (4.11E-10 kg/m^3, in column 11 of Table 4) is at Venus, or n=4 with r_n = 1.00E+11 m. The result is plotted in Figure 4a (in square markers).

Then, we try to use a single n valued r^2 * |R(n,*l*)|^2 * |Y(*l*,m)|^2 curve to describe the mass density r-distribution in the {1,n=1..6} region which include all four rocky planets (despite that {1,n=1..2//6} has zero mass). Here we cannot use {0,1//6} as n=1 due to it will give a too narrow probability curve to cover all region of {1,n=1..6}. As learned from Figure 3, if we use {1,1//6} as r_1 and n=1, it will generate much broad curve than that using {0,1//6} as r_1 and n=1. Since the mass density curve maximum at Venus n=4, we know it must be n=4's r^2 * |R(n,*l*)|^2 * |Y(*l*,m)|^2. Under the nLL QM effect (because {1,n=1..6} region is disk-lyzed), *l* = n-1 =3. Furthermore, here we only consider the radial mass distribution, so |Y(*l*,m)|^2 can be ignored for the moment. So in Table 5 (left), we used {1,1//6} as r_1 and n=1 to calculate r^2 * |R(n=4,*l*=3)|^2 curve. Using eq-5 and with the maximum value at n=4 and r_n = 1.00E+11, column 3 of Table 5 (left) was calculated as

$$r^2 *|R(4,3)|^2 \propto [r/1.00E+11 * \exp(1 - r/1.00E+11)]^{(2*4)} \qquad \text{eq-15}$$

After re-scale the value to the mass density (see column 4 of Table 5's left table), it fits to the {1,n=3..6} region's (Mercury, Venus, Earth, and Mars) mass density data perfectly (see Figure 4a solid line). Therefore, under the {N,n//q} QM, the mass distribution of four rocky planets (or the N=1 super shell space) in r-dimension is at |4,3,3> QM state with r_1 at {1,1//6}. Or, |4,3,3> QM state with r_1 at {1,1//6} is the Eigen description of N=1 super shell's mass distribution in r-dimension.

Similarly, we try to use a single n valued r^2 * |R(n,*l*)|^2 * |Y(*l*,m)|^2 curve to describe the mass density r-distribution in the {2,n=1..6} region. Using {2,1//6} as r_1 and n=1 for region {2,n=1..6}, the mass density curve maximum at Jupiter n=2, so we know it must be r^2 * |R(n=2,*l*=1)|^2. Using eq-5 and with the maximum value at n=2, or $r = r_1 * (n*5.33/6)^2 = r_1 * (r/r_1) * (5.33/6)^2$, column 3 of Table 5 (middle-left table) was calculated as

$$r^2 *|R(2,1)|^2 \propto [r/7.12E+11 * \exp(1 - r/7.12E+11)]^{(2*2)} \qquad \text{eq-16}$$

After re-scale the value to the mass density (see column 4 of Table 5's middle-left table), it fits to the {2,n=1..6} region's (Mars, Jupiter, Saturn, Uranus, Neptune, and Kuiper belt) mass density data reasonable well (see Figure 4a dash line). Therefore, under the {N,n//q} QM, the mass distribution of four gas/ice planets (or the N=2 super shell) in r-dimension is at the |2,1,1> QM state with r_1 at {2,1//6}. Or, |2,1,1> QM state with r_1 at {2,1//6} is the Eigen description of N=2 super shell's mass distribution in r-dimension.

Now, if we want to use a single n valued r^2 * |R(n,*l*)|^2 * |Y(*l*,m)|^2 curve to describe the mass density r-distribution in Solar system's whole {N=1..4,n} region, then we can move the r_1 even outward to {3,1//6}, or {4,1//6}, etc., and then the r^2 * |R(n,*l*)|^2 curve will cover more broad r region. In Table 5 (middle-right table), {3,1//6} was used as the r_1. Since the maximum probability is at {1,4//6}, so it need to transform {1,4//6} ={2,4/6//6} ={3,4/6^2//6}, or n= 4/6^2 = 1/9. Now the probability function become r^2 *|R(n=4/6^2,*l*=n-1|^2. Using eq-5 and with the maximum value at n=4/6^2, or r = r_1 * (n*5.33/6)^2 = r_1 * (r/r_1) * (5.33/6)^2, column 3 of Table 5 (middle-right table) was calculated as

$$r^2 *|R(n=4/6^2,l=n-1)|^2 \propto [r/1.00E+11 * \exp(1 - r/1.00E+11)]^{(2/9)} \qquad \text{eq-17}$$

After re-scale the value to the mass density (see column 4 of Table 5's middle-right table), it fits to the {N=1..4,n} region's mass density data reasonably well (maximum point at Venus, heavy weighted points at Jupiter, Saturn, and Uranus, rather than Earth and Mars, see Figure 4a dotted line). Therefore, under the {N,n//q} QM, the mass distribution in the whole {N=1..4,n} region of the Solar system is at the Eigen QM state of |n=4/6^2,*l*=n-1,m=n-1> , with r_1 at {3,1//6}. Of course, this is a very low resolution description which ignored many (low weighted) details like Earth, Mars, Mercury, etc.

Table 4. Using {N,n//6} QM model to calculate the current mass density r-distribution in Solar system's {N=1..4,n} region.

NASA's data of planets			assigned N, n, period factor			set total n=1 at Sun core using {N,n} to calc total n & r					
	mass	Sun's radius or planets' $r_{n\text{-orbit}}$	N	n	period factor	total n from Sun core	calc. $r_{n\text{-orbit}}$= $n^2\ r_{1\text{-orbit}}$	r/r1=n^2	Original D=4.37E+28 /r^3.279	current avg. mass density	calc. $r_{n\text{-orbit}}$= $n^2\ r_{1\text{-orbit}}$
unit	kg	m					m	m/m	kg/m^3	kg/m^3	AU
Sun core		1.74E+08	0	1	6.75	1	***1.74E+08***	1	4.17E+01		0.00
SUN	1.989E+30	6.96E+08	0	2	6	2	6.96E+08	4	4.43E-01		0.00
{0,3} corona			0	3	6	3	1.57E+09	9	3.10E-02		0.01
{0,4} corona			0	4	6	4	2.78E+09	16	4.70E-03		0.02
{0,5} corona			0	5	6	5	4.35E+09	25	1.09E-03		0.03
{0,6} corona end			0	6	6	6	6.26E+09	36	3.29E-04		0.04
{1,2}			1	2	6	12	2.50E+10	144	3.49E-06		0.17
Mercury	3.3E+23	5.79E+10	1	3	6	18	5.64E+10	324	2.44E-07	9.53E-11	0.38
Venus	4.87E+24	1.08E+11	1	4	6	24	1.00E+11	576	3.71E-08	4.11E-10	0.67
Earth	5.97E+24	1.49E+11	1	5	6	30	1.57E+11	900	8.58E-09	1.87E-10	1.05
Mars	6.42E+23	2.28E+11	1	6	6	36	2.25E+11	1296	2.59E-09	8.80E-12	1.51
Jupiter	1.898E+27	7.78E+11	2	2	5.33	64.0	7.12E+11	4.09E+03	5.99E-11	1.21E-10	4.78
Saturn	5.68E+26	1.43E+12	2	3	5.33	95.9	1.60E+12	9.20E+03	4.19E-12	7.16E-12	10.7
Uranus	8.68E+25	2.97E+12	2	4	5.33	127.9	2.85E+12	1.64E+04	6.35E-13	3.19E-13	19.1
Neptune	1.02E+26	4.51E+12	2	5	5.33	159.9	4.45E+12	2.56E+04	1.47E-13	1.39E-13	29.8
Pluto	1.46E+22	5.91E+12	2	6	5.33	191.9	6.40E+12	3.68E+04	4.45E-14	4.31E-16	43.0
{3,2}			3	2	6	383.8	2.56E+13	1.47E+05	4.72E-16		172
{3,3}			3	3	6	575.6	5.76E+13	3.31E+05	3.31E-17		387
{3,4}			3	4	6	767.5	1.02E+14	5.89E+05	5.01E-18		688
{3,5}			3	5	6	959.4	1.60E+14	9.20E+05	1.16E-18		1074
Inner Oort, start 2000AU			3	6	6	1151.3	2.31E+14	1.33E+06	3.51E-19		1547
Inner Oort			4	2	6	2302.6	9.22E+14	5.30E+06	3.72E-21		6189
Inner Oort, end 20000AU			4	3	6	3453.8	2.07E+15	1.19E+07	2.61E-22		13925
outer Oort, start 20000AU			4	4	6	4605.1	3.69E+15	2.12E+07	3.95E-23		24755
outer Oort			4	5	6	5756.4	5.76E+15	3.31E+07	9.15E-24		38679
outer Oort,end 50000AU			4	6	6	6907.7	8.30E+15	4.77E+07	2.77E-24		55698

Note: in column 11, current averaged mass density = mass /[4/3* π*(r_{n+1}^3 - r_n^3)]. Mars outer range is calculated as Mars orbit-r times (7/6)^2. So does for Kuiper belt's outer range. Note: Kuiper belt's mass is assumed to be 5x of Earth's mass.

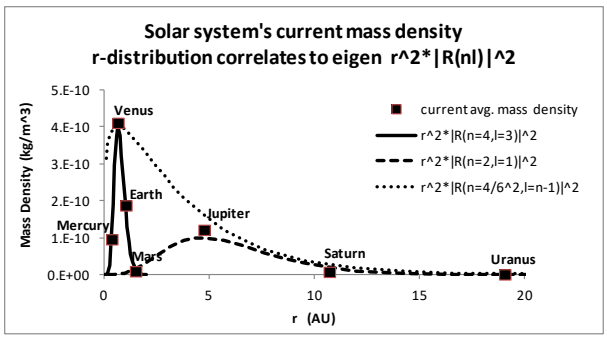

Figure 4a. Solar system's current mass density r-distribution correlates to its Eigen r^2*|R(n,*l*)|^2 probability curve.

Table 5. Using r^2 * |R(n,*l*)|^2 curve and eq-5 to fit to the mass density r-distribution in Solar system {N=1..4,n} regions.

based on {1,1//6}, max at {1,4//6} or n=4

max.prob. n=		4	
r_1 at		{1,1//6}	
r_1=		6.26E+09	m
Prob. Scaling factor =			4.00E-10
r/r_1=	r= r/r1*r1, AU	r^2*|R(n=4,l=3)|^2	r^2*|R(n=4,l=3)|^2
0.4	0.02	3.79E-10	1.52E-19
2.4	0.10	2.34E-04	9.35E-14
4	0.17	6.24E-03	2.50E-12
6	0.25	5.87E-02	2.35E-11
8	0.34	2.15E-01	8.61E-11
10	0.42	4.71E-01	1.88E-10
12	0.50	7.43E-01	2.97E-10
14	0.59	9.36E-01	3.74E-10
16	0.67	1.00E+00	4.00E-10
18	0.76	9.42E-01	3.77E-10
20	0.84	8.03E-01	3.21E-10
22	0.92	6.32E-01	2.53E-10
24	1.01	4.65E-01	1.86E-10
26	1.09	3.24E-01	1.30E-10
28	1.18	2.15E-01	8.61E-11
30	1.26	1.37E-01	5.49E-11
32	1.35	8.44E-02	3.37E-11
36	1.51	2.92E-02	1.17E-11
40	1.68	9.13E-03	3.65E-12
44	1.85	2.64E-03	1.05E-12
48	2.02	7.12E-04	2.85E-13

r1 at {2,1//6}, max at {2,2//6} or n=2

max.prob. n=		2	
r_1 at		{2,1//6}	
r_1=		2.26E+11	m
Prob. Scaling factor =			1.00E-10
r/r_1=	r= r/r1*r1*(5.33/6)^2, AU	r^2*|R(n=2,l=1)|^2	r^2*|R(n=2,l=1)|^2
0.2	0.24	2.79E-04	2.79E-14
0.4	0.48	3.66E-03	3.66E-13
0.6	0.72	1.52E-02	1.52E-12
0.8	0.96	3.92E-02	3.92E-12
1	1.19	7.84E-02	7.84E-12
1.2	1.43	1.33E-01	1.33E-11
1.4	1.67	2.02E-01	2.02E-11
1.6	1.91	2.82E-01	2.82E-11
1.8	2.15	3.70E-01	3.70E-11
2	2.39	4.62E-01	4.62E-11
2.2	2.63	5.53E-01	5.53E-11
2.4	2.87	6.42E-01	6.42E-11
2.6	3.11	7.24E-01	7.24E-11
2.8	3.34	7.97E-01	7.97E-11
3.2	3.82	9.11E-01	9.11E-11
3.6	4.30	9.79E-01	9.79E-11
4	4.78	1.00E+00	1.00E-10
4.8	5.73	9.32E-01	9.32E-11
5.6	6.69	7.76E-01	7.76E-11
6.4	7.64	5.95E-01	5.95E-11
7.2	8.60	4.28E-01	4.28E-11
8	9.55	2.93E-01	2.93E-11
10	11.94	9.70E-02	9.70E-12
12	14.33	2.72E-02	2.72E-12
14	16.72	6.83E-03	6.83E-13
16	19.11	1.58E-03	1.58E-13
18	21.50	3.42E-04	3.42E-14
20	23.89	7.06E-05	7.06E-15

r1 at {3,1//6}, max at {1,4//6} or n=4/6^2=1/9

max.prob. n=		1/9	
r_1 at		{3,1//6}	
r_1=		8.12E+12	m
Prob. Scaling factor =			4.00E-10
r/r_1=	r= r/r1*r1*(5.33/6)^2, AU	r^2*|R(n=4/6^2,l=n-1)|^2	r^2*|R(n=4/6^2,l=n-1)|^2
0.0022	0.10	7.85E-01	3.14E-10
0.0044	0.19	8.87E-01	3.55E-10
0.0067	0.29	9.40E-01	3.76E-10
0.0089	0.38	9.71E-01	3.88E-10
0.0111	0.48	9.89E-01	3.95E-10
0.0133	0.57	9.97E-01	3.99E-10
0.0156	0.67	1.00E+00	4.00E-10
0.0178	0.76	9.98E-01	3.99E-10
0.0222	0.96	9.84E-01	3.94E-10
0.0333	1.43	9.20E-01	3.68E-10
0.0444	1.91	8.37E-01	3.35E-10
0.0556	2.39	7.51E-01	3.00E-10
0.0667	2.87	6.67E-01	2.67E-10
0.0778	3.34	5.90E-01	2.36E-10
0.0889	3.82	5.19E-01	2.07E-10
0.1111	4.78	3.97E-01	1.59E-10
0.1333	5.73	3.01E-01	1.21E-10
0.1556	6.69	2.27E-01	9.09E-11
0.1778	7.64	1.71E-01	6.83E-11
0.2222	9.55	9.53E-02	3.81E-11
0.2778	11.94	4.54E-02	1.82E-11
0.3333	14.33	2.14E-02	8.57E-12
0.3889	16.72	1.01E-02	4.02E-12
0.4444	19.11	4.70E-03	1.88E-12
0.5556	23.89	1.01E-03	4.06E-13
0.6667	28.66	2.17E-04	8.69E-14
0.8889	38.22	9.79E-06	3.92E-15
1.1111	47.77	4.35E-07	1.74E-16

r1 at {1,1//6}, max at {1,2//6} or n=2

max.prob. n=		2	
r_1 at		{1,1//6}	
r_1=		6.26E+09	m
Prob. Scaling factor =			4.00E-06
r/r_1=	r/r1*r1, AU	r^2*|R(n=2,l=1)|^2	r^2*|R(n=2,l=1)|^2
1/5	0.01	2.82E-04	1.13E-09
0.4	0.02	3.69E-03	1.48E-08
0.6	0.03	1.53E-02	6.11E-08
0.8	0.03	3.95E-02	1.58E-07
1	0.04	7.90E-02	3.16E-07
1.2	0.05	1.34E-01	5.36E-07
1.4	0.06	2.03E-01	8.13E-07
1.6	0.07	2.84E-01	1.13E-06
1.8	0.08	3.72E-01	1.49E-06
2	0.08	4.64E-01	1.86E-06
2.2	0.09	5.56E-01	2.22E-06
2.4	0.10	6.44E-01	2.58E-06
2.6	0.11	7.26E-01	2.90E-06
2.8	0.12	7.99E-01	3.20E-06
3.2	0.13	9.13E-01	3.65E-06
3.6	0.15	9.80E-01	3.92E-06
4	0.17	1.00E+00	4.00E-06
4.8	0.20	9.30E-01	3.72E-06
5.6	0.24	7.73E-01	3.09E-06
6.4	0.27	5.91E-01	2.37E-06
7.2	0.30	4.25E-01	1.70E-06
8	0.34	2.90E-01	1.16E-06
10	0.42	9.55E-02	3.82E-07
12	0.50	2.67E-02	1.07E-07
14	0.59	6.66E-03	2.66E-08
16	0.67	1.53E-03	6.12E-09
18	0.76	3.30E-04	1.32E-09
20	0.84	6.79E-05	2.71E-10

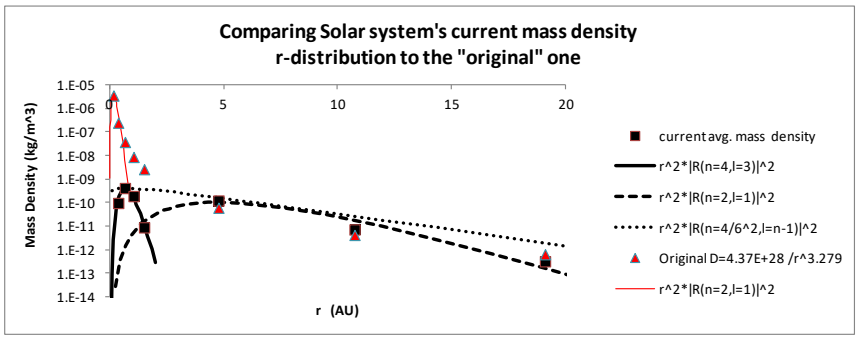

Figure 4b. Comparing Solar system's current mass density r-distribution to the "original" one.

In Figure 4b, we try to compare Solar system's current mass density r-distribution (that was shown in Figure 4a) to the original mass density r-distribution to see how it has evolved. The "original" mass density r-distribution was calculated in paper SunQM-1s1 Table 3b, and copied to current paper's Table 4 column 10, and presented in Figure 4b as red triangle markers. Notice that the y-axis in Figure 4b is in log scale. According to what we learned from Figure 4a, this initial mass density r-distribution should able to be described by a single valued n's r^2 * |R(n,*l*)|^2 * |Y(*l*,m)|^2 curve with r_1 at {1,1//6}, and maximum probability at n=2 of {1,2//6} (like that in the current {2,n=1..6//6} region). This probability curve was calculated in the Table 5 (right), and plotted in Figure 4b as red solid line. We can see that the r^2*|R(2,1)|^2 curve fits roughly only the {1,n=2..4//6} region, not the {1,n=5..6//6} region of the red-triangle markers. So if we expect a single n r^2*|R(2,1)|^2 curve to represent the initial stage of mass density r-distribution in {1,n=1..6//6}, then the red-triangle marks should be explained as the sum of many n(s) of r^2*|R(n,n-1)|^2 curves with n= 2, 3, 4, 5, and 6 (and the higher the n, the lower the weight in the sum). In other words, the log-log linear fitting in SunQM-1s1 only generated one of the early stages (but not the earliest) of mass density r-distribution. It correlates to a combination of |2,1,1>, |3,2,2>, |4,3,3>, |5,4,4>, and |6,5,5> QM states (with r_1 at {1,1//6}) with decreasing weights. There probably was an earlier stage than that, which was a single n |2,1,1> QM state (with r_1 at {1,1//6}) which could form a Jupiter-sized planet at {1,2//6} orbit, or with r = 0.17 AU. In wiki "Hot Jupiter" figure "*Hot Jupiters (along left edge, including most of planets detected using the transit method, indicated with black dots) discovered up to 2 January 2014*", many hot Jupiters have been found at r range from 0.04 AU (which close to {1,1//6} orbit) to 1.1 AU. It strongly suggests that the |1,0,0> QM state (with r_1 at {1,1//6}) may be the even earlier QM state than the |2,1,1> QM state for the mass density r-distribution in the very early Solar system. However, if the "ball-torus-7-11-gap effect" (see SunQM-1s1) is correct, then the peak of mass density r-distribution is unlikely to be at {1,1//6}, but more likely to be at {1,2//6}.

So, with above analysis, an imagined story of how our Solar system {N=1..4,n} region's mass density r-distribution was evolved is presented below (Notice that most of the explanation below come from Wikipedia and contributed by other scientists. I only add the {N,n} QM result into the explanation): after the pre-Sun nebula quantum collapsed from {6,1} to {5,1}, {4,1}, {3,1}, {2,1}, {1,1}, and then to {0,2}, > 99% mass fell into the {0,2} current Sun ball, and < 1% mass leftover in the {N=1..4,n} space region. Meanwhile, the spinning Sun's nLL QM effect caused the leftover mass to disk-lyze, and the disk-lyzed mass in {N=1..4,n} region now can be described by radial wave function's r^2 * |R(n,*l*)|^2 probability curve in either low, or median, or high resolution as shown in Figure 5a. Under a low resolution description, we can use a single n valued r^2 * |R(n=2,*l*=1)|^2 probability curve for the whole {N=1..4,n} region, with r_1 at {3,1//6} and maximum mass density at {1,2//6} (as shown in Table 5 (middle-right) but with maximum probability at {1,2//6} not {1,4//6}, or an illustration in Figure 5a grey line curve). Under a median resolution description, we can use a single n valued r^2 * |R(n,*l*)|^2 probability curve for each {N,n=1..6//6} super shell region, with r_1 at {N,1//6} and maximum mass density at {N,2//6} (as shown in Figure 5a dashed line curve). Under a high resolution description, we need to use every n in {N=1..4,n//6} region, each n for a r^2 * |R(n,*l*)|^2 probability curve, with r_1 at {0,1//6} and maximum mass density at {N,n//6} (as shown in Figure 1a for Asteroid belt, or Figure 2b for Kuiper belt, or an illustration in Figure 5a's solid line curves). Note: again, that the maximum mass density at {N,2//6} is due to the "ball-torus-7-11-gap effect". If there is no this effect, then the max should be at {N,1//6}.

Then the outward migration of mass (driven by the expansion of rock-evap-line and ice-evap-line) in Solar system's {N=1..4,n} region before and after Figure 5a's initial stage can be illustrated in Figure 5b. In Figure 5b, stage 1 curve is the possible mass density r-distribution before Figure 5a's "original" stage. Stage 2 curve is close to the "original" stage (the log-log linear curve in SunQM-1s1's fitting). Stage 3 is the current state of mass density r-distribution in Solar system's {N=1..4,n} region. Stage 4 is the possible future state of mass density r-distribution in Solar system's {N=1..4,n} region. Note: Data for Figure 5a and for Figure 5b are not shown here because the data was artificially built, not calculated out.

One thing worthwhile to mention is that for the log-log linear fitted model of "original" Venus and Earth (with 42x and 25x of current Earth's mass, see SunQM-1s1 Table 3b column 12), there are three possibilities: 1) They might really formed in the early time, so both Venus and Earth had a ~18000 km thick "original" atmosphere (made of H/He/ice) which was then stripped off after the ice-evap-line expansion passed {1,6//6}; 2) They never formed, or the ice-evap-line expansion had already passed {1,n=3..4//6} and all H/He/ice within that region had already evaporated before the accretion of Venus and Earth, so that Venus and Earth accreted in sizes as that of today; 3) in between possibility 1) and 2). If possibility 2) is correct, then the log-log linear fitted model of "original Venus and Earth" is only a projection for the case that if there were

no ice-evap-line expansion. Unfortunately, {N,n} QM alone can't tell which one among three possibilities is correct. Only thing we know is that possibility 1) is unlikely to be correct for Mercury. This is because Mercury orbit's high inclination and high eccentricity implies that Mercury accreted only part of mass in the whole orbit space of {1,3//6}o (like that of Pluto), even General Relativity's precession have made some significant effect.

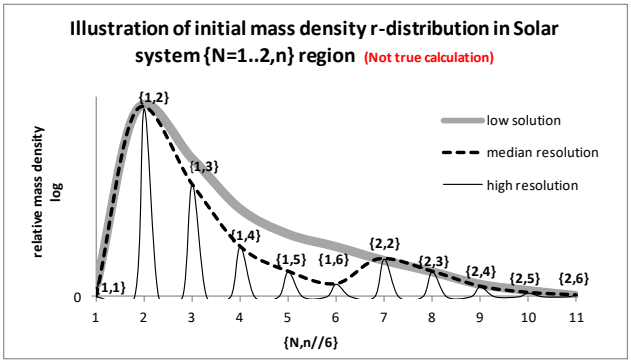

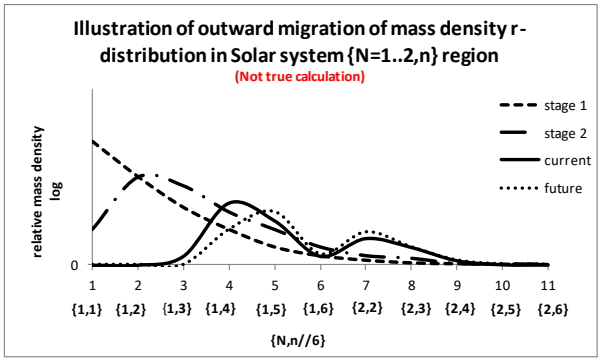

Figure 5a (left). Illustration of a possible initial mass density r-distribution in Solar system's {N=1..2,n} region. Note: these curves are artificially drawn to mimic the r^2 * |R(n,*l*)|^2 calculated curve, they are not the true calculated result.
Figure 5b (right). Illustration of a possible outward migration of mass density r-distribution in Solar system's {N=1..2,n} region (driven by the expansion of rock-evap-line and ice-evap-line). Note: these curves are artificially drawn to mimic the r^2 * |R(n,*l*)|^2 calculated curve, they are not the true calculated result.

VII. Saturn ring (and Jupiter ring) re-analyzed by using r^2*|R(n,*l*=n-1)|^2 curve

The newly developed method (in section II of current paper) is valid not only for belts in the Sun-planet/belt system, but also for the rings in planet-moon/ring system. So now we apply this method to both Saturn's ring and Jupiter's ring (even though they have been analyzed in SunQM-3s4 using the old method). Table 6a shows the Saturn's ring data (which is obtained from wiki "Rings of Saturn", also see Table 1 of SunQM-3s4). Using Saturn's Earth-sized core as pCore{0,1//3} and r_1, its ABCD rings are at pCore{0,4//3}o orbit space. Using n=4, we can calculate the normalized r^2 *|R(4,3)|^2 curve by using eq-5. The calculated result is shown in Table 6b (left table, with ABCD rings being assigned with blue, green yellow and pink colors respectively), and plotted in Figure 6 (short-dashed line). From Figure 3 of SunQM-3s4, we guessed that the relative radial mass density of ABCD rings are around 50%, 100%, 50%, and 10%. So Figure 6 short-dash line curve is obvious too wild to fit rings ABCD. To make a narrower probability curve, we need to shift r_1 further inward. Notice that inside Earth-sized core, Saturn has a {N,n//2} QM structure. After translating Saturn's QM structure into a {N,n//2}, Saturn's ABCD ring is now at pCore{2,1//2} = pCore{0,4//2}, Saturn's surface at pCore{0,3//2}, Saturn's Earth-sized core at pCore{0,1//2}. So we shift r_1 to further inward to pCore{-1,1//2}, or to pCore{-2,1//2}, or even to pCore{-3,1//2}, and then the ABCD rings (or the maximum mass density) are at either pCore{-1,8//2}, or pCore{-2,16//2}, or pCore{-3,32//2} respectively, or with n= 8, 16, or 32, respectively. The r^2 * |R(n,*l*=n-1)|^2 calculation was done in Table 6 (middle-left), (middle-right) and right respectively. The resulted curves are plotted in Figure 6 as dash-dot line, solid line, and dot line respectively. It is obvious that the n=16 curve r^2 * |R(16,15)|^2 give the best fitting. Therefore, Saturn's ABCD rings can be best described by an Eigen radial probability density curve r^2 * |R(16,15)|^2 with r_1 at pCore{-2,1//2}, and the ABCD rings at pCore{-2,16//2} QM structure.

Also Saturn ring's width Δr must be evolved from wild to narrow, or from low n to high n, likely from n=4, to n=8, to current n= 16, then to further n=32, as shown in Figure 6b. It is naturally to think that as the width of the ring narrowing, the peak will have higher mass density, and will more easily to trigger the accretion of moon.

Table 6a. Saturn's ring data obtained from wiki "Rings of Saturn".

	m
Saturn surface r	5.82E+07
D-ring, inner edge	6.69E+07
D-ring, outer edge	7.45E+07
C-ring, inner edge	7.47E+07
C-ring, outer edge	9.20E+07
B-ring, inner edge	9.20E+07
B-ring, outer edge	1.18E+08
A-ring, inner edge	1.22E+08
A-ring, outer edge	1.37E+08

Table 6b. Using normalized r^2 *|R(n,n-1)|^2 curve in eq-5 to fit Saturn ABCD rings mass density r-distribution.

A-ring ~80%, too high, Saturn's Earth-sized core as r1				A-ring ~65%, OK 1/4 Earth-sized core as r1				A-ring ~48%, best 1/4/4 Earth-sized core as r1				A-ring ~22%, too low 1/4/4/4 Earth-sized core as r1		
re-scale factor			0.3	re-scale factor			0.5	re-scale factor			0.7			
n=	4			n=	8			n=	16			n=	32	
r_1 at	pCore{0,1//2}			r_1 at	pCore{-1,1//2}			r_1 at	pCore{-2,1//2}			r_1 at	pCore{-3,1//2}	
r_1=	6.47E+06	m		r_1=	1.62E+06	m		r_1=	4.04E+05	m		r_1=	1.01E+05	m
r/r_1=	r^2*|R(4,3)|^2	(r/r1)*r1, m	re-scaled r^2*|R(4,3)|^2	r/r_1=	r^2*|R(8,7)|^2	(r/r1)*r1, m	re-scaled r^2*|R(8,7)|^2	r/r_1=	r^2*|R(16,15)|^2	(r/r1)*r1, m	re-scaled r^2*|R(16,15)|^2	r/r_1=	r^2*|R(32,31)|^2	(r/r1)*r1, m
1	0.00	6.47E+06	1.22E-07	1	0.00	1.62E+06	4.06E-23	1	0.00	4.04E+05	3.64E-64	1	0.00	1.01E+05
4	0.01	2.59E+07	1.80E-03	24	0.00	3.88E+07	1.61E-03	100	0.00	4.04E+07	1.63E-05	320	0.00	3.24E+07
6	0.06	3.88E+07	1.70E-02	28	0.01	4.53E+07	7.00E-03	121	0.00	4.89E+07	5.31E-04	384	0.00	3.88E+07
8	0.21	5.18E+07	6.28E-02	32	0.04	5.18E+07	2.19E-02	136	0.00	5.50E+07	3.46E-03	448	0.00	4.53E+07
9	0.33	5.82E+07	9.80E-02	36	0.11	5.82E+07	5.33E-02	151	0.02	6.11E+07	1.52E-02	512	0.00	5.18E+07
10	0.46	6.47E+07	1.38E-01	40	0.21	6.47E+07	1.06E-01	166	0.07	6.71E+07	4.88E-02	640	0.00	6.47E+07
11	0.60	7.12E+07	1.80E-01	44	0.36	7.12E+07	1.81E-01	181	0.17	7.32E+07	1.20E-01	704	0.02	7.12E+07
12	0.73	7.76E+07	2.20E-01	48	0.54	7.76E+07	2.69E-01	196	0.34	7.93E+07	2.37E-01	768	0.08	7.76E+07
13	0.85	8.41E+07	2.54E-01	52	0.71	8.41E+07	3.57E-01	211	0.56	8.53E+07	3.89E-01	832	0.26	8.41E+07
14	0.93	9.06E+07	2.79E-01	57	0.89	9.22E+07	4.47E-01	227	0.79	9.18E+07	5.51E-01	910	0.63	9.20E+07
15	0.98	9.71E+07	2.94E-01	60	0.96	9.71E+07	4.82E-01	241	0.94	9.75E+07	6.55E-01	960	0.86	9.71E+07
16	1.00	1.04E+08	3.00E-01	64	1.00	1.04E+08	5.00E-01	256	1.00	1.04E+08	7.00E-01	1024	1.00	1.04E+08
17	0.99	1.10E+08	2.96E-01	68	0.97	1.10E+08	4.87E-01	271	0.96	1.10E+08	6.69E-01	1088	0.90	1.10E+08
18	0.95	1.16E+08	2.84E-01	73	0.87	1.18E+08	4.37E-01	292	0.76	1.18E+08	5.35E-01	1170	0.58	1.18E+08
19	0.89	1.23E+08	2.67E-01	76	0.79	1.23E+08	3.95E-01	301	0.66	1.22E+08	4.61E-01	1216	0.39	1.23E+08
20	0.81	1.29E+08	2.44E-01	80	0.66	1.29E+08	3.31E-01	316	0.48	1.28E+08	3.38E-01	1280	0.19	1.29E+08
22	0.64	1.42E+08	1.93E-01	84	0.53	1.36E+08	2.67E-01	331	0.33	1.34E+08	2.31E-01	1344	0.08	1.36E+08
24	0.48	1.55E+08	1.43E-01	92	0.31	1.49E+08	1.57E-01	346	0.21	1.40E+08	1.47E-01	1408	0.03	1.42E+08
26	0.34	1.68E+08	1.01E-01	96	0.23	1.55E+08	1.14E-01	361	0.13	1.46E+08	8.87E-02	1472	0.01	1.49E+08
28	0.22	1.81E+08	6.72E-02	104	0.11	1.68E+08	5.62E-02	376	0.07	1.52E+08	5.05E-02	1536	0.00	1.55E+08
30	0.14	1.94E+08	4.32E-02	110	0.06	1.78E+08	3.10E-02	391	0.04	1.58E+08	2.73E-02	1792	0.00	1.81E+08
32	0.09	2.07E+08	2.67E-02	128	0.01	2.07E+08	3.97E-03	512	0.00	2.07E+08	4.41E-05	2048	0.00	2.07E+08

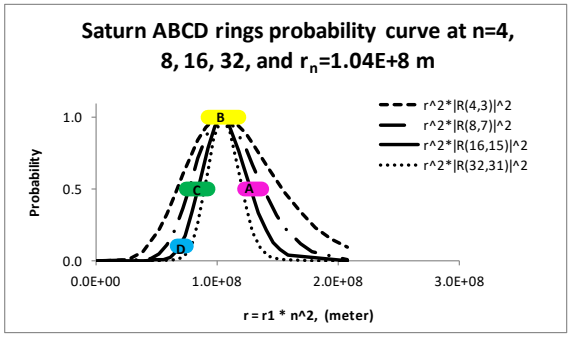

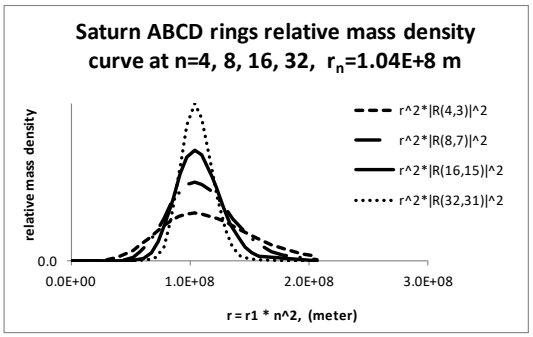

Figure 6a (left), Saturn ABCD rings' probability curve at n=4, 8, 16, 32, maximum probability at r_1 *n^2 =1.04E+8 m.
Figure 6b (right), Saturn ABCD rings' relative mass density curve at n=4, 8, 16, 32, maximum probability at r_1 *n^2 =1.04E+8 m.

Now let's use r^2 * |R(n,*l*=n-1)|^2 curve to analyze Jupiter's ring. Table 7a shows the Jupiter ring's data (which is obtained from wiki "Rings of Jupiter", also see Table 6 of SunQM-3s4). From Table 7a, the main ring has mass around E+11 to E+16 kg (all other rings' mass can be ignored), and Metis moon has mass 3.6E+16 kg (moon Adrastea's mass can also be ignored), So Metis has > 50% of total mass of inner moons and main ring. In Table 7b's calculation, similar as that for Saturn, Jupiter's Earth-sized core is at pCore{0,1//2}, Jupiter's surface is at {0,3//2}, Jupiter's ring is at {0,4//2} (see the discussion in SunQM-3s7 that Jupiter's {N,n//q} has superposition of q=5, 3, and 2).

In Table 7b (left), Jupiter ring's r^2 * |R(n,*l*=n-1)|^2 curve is calculated by using r_1 at pCore{-3,1//2}, or Jupiter ring is at n= 4*2^3 = 32. If use Jupiter's surface r at 6.99E+7 m, then r^2 * |R(n,*l*=n-1)|^2 curve's peak is always at 1.24E+8 m, not moon Metis' orbit r =1.29E+8 m. However, we want to set r^2 * |R(n,*l*=n-1)|^2 curve's peak at r =1.29E+8 m (because moon Metis must have collected > 50% of mass of Jupiter's main ring region from 0.92E+8 m to 1.82E+8 m). So we have to multiply a factor of 1.04 to 6.99E+7 m to make the probability curve peak at 1.29E+8 m. Therefore, r_1 = 6.99E+7 * 1.04 /3^2 / 2^2 / 2^2 / 2^2 = 1.26E+5 m, and maximum probability at r = r_1 *n^2 =1.26E+5 * 32^2 = 1.29E+8 m. The calculated r^2 *|R(32,31,)|^2 curve is plotted in Figure 7 as dash line. What we need is that Metis (in orbit space (1.29 ± 0.005)E+8 m) should have > 50% of total mass of inner moons and main ring (in Table 7b). Obviously the curve with n=32 is too broad, It has ~50% at around (1.29 ± 0.19)E+8 m (or from 1.11E+8 m to 1.49E+8 m, see Table 7b (left) columns 2 and 3). Again, according to Figure 3, to make a probability curve narrower, the r_1 needs to be move inward and n needs to be higher. After a search, it shows that n must be ≥ 8192, where r^2 *|R(8192,8191)|^2 probability curve decreased from 100% to ~60% at around (1.29 ± 0.01)E+8 m (see Table 7b (right)). This result fits to the hypothesis that the accretion of mass in a planet's ring (or in a star's belt) happens first at the peak of probability curve, and accompanied by the narrowing of the probability curve (in r-dimension, as shown in Figure 6b). In {N,n//q} QM, this is equivalent to that n' is increased to a higher value, or the r_1 is decreased to lower value (or collapsed inward). In the case of Figure 7, if we use Jupiter's Earth-sized core as the original r_1 pCore{0,1//2}, then its n'=8192 's r_1 is at pCore{0,1/2^(-11)//2} = pCore{-11,1//2}, and Jupiter's ring is at pCore{-11,4//2} orbit.

Table 7a. Jupiter ring's data obtained from wiki "Rings of Jupiter".

	mass, kg	r, m
Jupiter surface r		6.99E+07
Jupiter ring		
ring-1, Halo ring, inner edge	E+7~E+9	9.20E+07
ring-1, Halo ring, outer edge		1.23E+08
ring-2, Main ring, inner edge	E+11~E+16	1.23E+08
ring-2, Main ring, outer edge		1.29E+08
ring-3, Amalthea gossamer ring, inner edge	E+7~E+9	1.29E+08
ring-3, Amalthea gossamer ring, outer edge		1.82E+08
ring-4, Thebe gossamer ring, inner edge	E+7~E+9	1.29E+08
ring-4, Thebe gossamer ring, outer edge		2.26E+08
Jupiter (inner) minor moons		
Metis, 4-1 moon	3.60E+16	1.29E+08
Adrastea, 4-2 moon	2.00E+15	1.29E+08

Table 7b. Using normalized r^2 *|R(n,n-1)|^2 curve to fit Jupiter ring's mass density r-distribution. Moon Metis' r (=1.29E+8 m) is marked in yellow.

n=	32	
r_1 at	{-3,1//2}	
r1 factor	1.04	
r_1=	1.26E+05	m
r/r_1=	r^2*|R(32,31)|^2	(r/r1)*r1, m
1	0.00	1.26E+05
512	0.00	6.46E+07
640	0.00	8.08E+07
704	0.02	8.89E+07
768	0.09	9.69E+07
832	0.28	1.05E+08
878	0.50	1.11E+08
960	0.88	1.21E+08
1024	1.00	1.29E+08
1088	0.88	1.37E+08
1180	0.50	1.49E+08
1216	0.36	1.53E+08
1280	0.17	1.62E+08
1344	0.07	1.70E+08
1408	0.03	1.78E+08
1472	0.01	1.86E+08
1536	0.00	1.94E+08
1600	0.00	2.02E+08
1664	0.00	2.10E+08
1728	0.00	2.18E+08
1792	0.00	2.26E+08
2048	0.00	2.59E+08

n=	8192	
r_1 at	{-11,1//2}	
	1.04	
r_1=	1.93E+00	m
r/r_1=	r^2 *|R(8192,8191)|^2	(r/r1)*r1, m
4.19E+07	0.00	8.08E+07
6.19E+07	0.00	1.19E+08
6.29E+07	0.00	1.21E+08
6.40E+07	0.00	1.23E+08
6.50E+07	0.00	1.25E+08
6.55E+07	0.02	1.26E+08
6.61E+07	0.21	1.27E+08
6.66E+07	0.76	1.28E+08
6.70E+07	1.00	1.29E+08
6.76E+07	0.46	1.30E+08
6.82E+07	0.08	1.31E+08
6.87E+07	0.01	1.32E+08
6.92E+07	0.00	1.33E+08
6.97E+07	0.00	1.34E+08
7.03E+07	0.00	1.35E+08
7.08E+07	0.00	1.36E+08
7.13E+07	0.00	1.37E+08
7.18E+07	0.00	1.38E+08
7.24E+07	0.00	1.39E+08
7.29E+07	0.00	1.40E+08
1.17E+08	0.00	2.26E+08
1.34E+08	0.00	2.59E+08

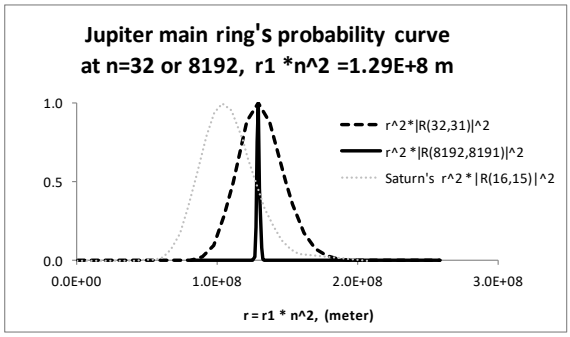

Figure 7. Jupiter main ring (including moons of Metis and Adrastea)'s probability curve at n=32 or 8192, maximum at r_1 *n^2 =1.29E+8 m. The grey dotted curve is a reference curve using Saturn ABCD rings r-dimension width and maximum at r = 1.04E+8 m and n=16.

VIII. More discussions

1) Schrodinger equation is a matter wave equation, so Solar system's radial mass density distribution can be described by a wave function, either in low solution, or in high resolution.

2) We need to point out that the rule of "all mass between r_n and r_{n+1} belongs to orbit n" is relatively accurate for the ~100% mass occupancy. For < 1% mass occupancy, the mass will form belt (or ring) under spinning QM's nLL effect, with the maximum radial mass density at r_n, and roughly equal range of Δr on both side of r_n, so that the belt (or ring) has width of $r_n \pm \Delta r$.

3) Figure 4a tells us that according to QM probability fitting, Mars at {1,6} was originally much smaller than what was fitted in the log-log-linear model (in SunQM-1s1). In a recent PBS-NOVA TV program "The Planets: Jupiter" [17], some scientists explained why Mars has such small mass as because the early Jupiter had a inward migration that cleared out the mass in {1,n=6..11/6}o orbit shell space. In the solar {N,n} QM model, this is caused by the "7-11 ball-torus gap effect". Actually it

should be called "6-11 ball-torus gap effect". Mars' low mass is due to that all {1,6}o orbit shell mass was cleared out by the "6-11 ball-torus gap effect". However, at the out edge of {1,5//6}o pre-Sun ball, there was small amount of mass in |nlm> = |6,5,5> QM mode, and it was structured as a belt that embedded on the surface of {1,5//6}o orbit shell (see the similar structure in Figure 4 of SunQM-3s3, where a |5,4,4> mode is embedded on Jupiter {0,4//5}o orbit shell's |4,0,0> surface). After the pre-Sun ball's {N=1,n=1..5}o super shell collapsed, this small amount of |6,5,5> mode (may be a collection of |6,5,m=-5…+5> QM modes) mass was retained at {1,6//6}o orbit and eventually formed a small massed Mars. Then, the expansion of ice-evap-line drove the r-dimension's ice/H/He density peak from around {1,1//6} moving outward (like a ring stain). As this peak approaching to Mars' orbit {1,6//6}, the mass of Mars kept increasing by capturing this out-flying ice/H/He peak. So once upon time, Mars' mass could have reached close to 19x times of current Earth mass (as shown in SunQM-1s1 Table 3b), most of the mass was ice/H/He. Then, after the ice-evap-line passed {1,6//6} and to today's around {1,9//6}, Mars lost not only all captured ice/H/He, but also all of its original atmosphere.

4) We need to emphasize that the Kuiper belt collected all mass in {2,6//6}o orbit shell space up to {2,7//6}. Using {0,1//6} as r_1, it contains {N=0,n=192..224//6}, or |n=192..224, *l*, m>, or over hundreds of possible QM (sub-)states (if considering different n, *l*, and m quantum numbers). However, due to the leftover mass is so little, among hundreds possible QM states, all mass takes only the lowest (or Eigen) QM state energy state |192,191,m> in r-dimension! This is also true for the Asteroid belt: among all |n=48..54, *l*,m> QM sub-states, all Asteroid bell's mass takes the single lowest (or Eigen) QM state energy state |48,47,47> in both r- and θ-dimensions.

5) While Kuiper belt takes the lowest r-dimensional energy state |192,191,m>, the cold-KBO (a major population in Kuiper belt) takes the lowest energy state |192,191,191> in both r- and θ-dimensions. Since the cold-KBO contains small objects with low orbital inclinations and eccentricities, it is more likely that the cold-KBO (rather than the whole Kuiper belt which contains those dwarf planets like Pluto, Haumea, Makemake, etc.) is the true "ring stain" of the current out-flying methane-ice mixture fragments driven by the expansion of methane-evap-line (or the solar wind stop line). If this is true, then after the solar-wind-stop-line further expanding from current {3,1//6} = {2,6//6} to {2,7//6}, the cold-KBO belt will out-moving to {2,7//6} also, and Pluto will stay at {2,6//6}. In this way, the future Plute (at {2,6//6}) is more like today's Mars (at {1,6//6}), and the future cold-KBO belt is more like today's Asteroid belt. For the same reason, like that of Mars, Pluto (and Haumea, Makemake, etc.)'s mass is most likely come from the leftover mass of |6,5,5> QM mode after a {3,1//6} sized pre-Sun ball quantum collapsed to {2,1//6}. Also like that of Asteroid belt, the cold-KBO's mass is most likely come from inside the {3,n=1..5//6}o orbit space.

6) Notice that so far there were three major phases of mass migration in Solar system evolution history: First, a pre-Sun ball quantum collapsed from {6,1} to {0,2} with > 99% of mass migrated inward in r-dimension; Second, the leftover (< 1%) mass in {N=1..4,n} spherical space disk-lyzed so that all leftover mass migrated to $\theta \approx \pi/2$ in θ–dimension; Third, the leftover and disk-lyzed (< 1%) mass in {N=1..4,n} region is now migrating outward (driven by the expansion of the rock-evap-line, ice-evap-line, and methane-evap-line).

7) Here is a list of current Solar system's evap-lines (or stop-lines): rock-evap-line (or heavy atom evap-line) passed {1,2} so that {1,2} planet (including its core made of iron or other heavy atoms) completely evaporated. Light atom evap-line passed {1,3} closing to {1,4} so Mercury already lost most of its light elements (C, O, Mg, etc.) and Venus starts to lost CO_2[10]. Ice-evap-line passed {1,8}, so that Asteroid belt's ice has all evaporated. Methane-evap-line (or Solar wind stop line) stops just before the {2,6}, so all methane-ice mixture fragments are dumped in {2,6}o orbit shell as Kuiper belt. In a recent PBS-NOVA TV program [18] and an article in Scientific American [19], some scientists proposed that "*Because the sun has grown more luminous over time, the boundaries of the habitable zone in the solar system have shifted outward*". It matches our result from Solar {N,n} QM's study. Further away, {3,6} = {4,1} is the nLL force stop line. Beyond this line, Sun's G-forced QM produced nLL effect is overcome by the interstellar wind's effect. {4,6} = {5,1} is the Sun's G-forced bound force stop line. Beyond this line, an object is no longer bound to (or orbit to) Solar system. {5,6} = {6,1} is proposed to be the Sun's G-

forced unbound force stop line. Beyond this line, object's movement is no longer affected by the Sun. An updated Solar {N,n} QM structure periodic plot is shown in Figure 8.

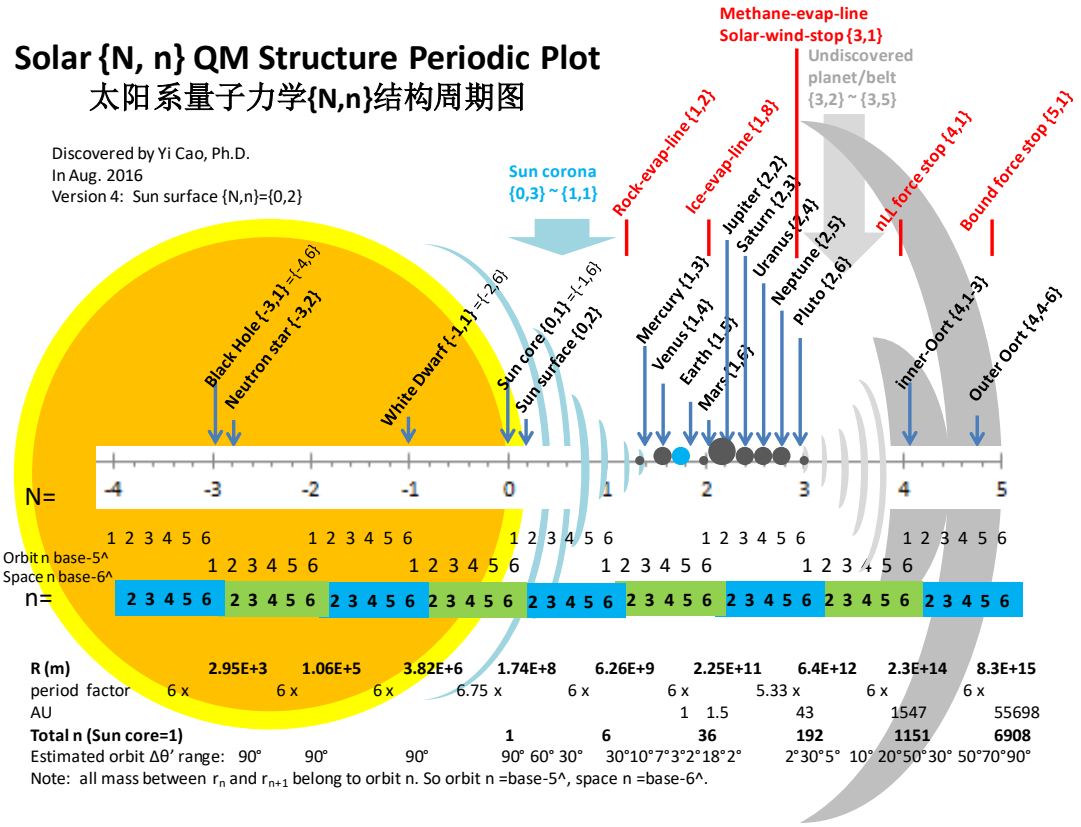

Figure 8. An updated Solar {N,n} QM structure periodic plot

8) Saturn ABCD rings have (r-dimensional) r_1 at pCore{-2,1//2}, Jupiter ring has (r-dimensional) r_1 at pCore{-11,1//2}, so different gas planet has different r_1 for their rings (even they have pretty much same Earth-sized core). Saturn's ABCD rings, E ring, F ring, G ring, etc. seem also have different r_1(s) for their r-dimensional Eigen description.

Conclusion

Just like Asteroid belt was explained as a "ring stain" of the once out-flying ice-rock mixture fragments (driven by the fast expansion of the ice-evap-line), the cold-KBO of Kuiper belt is also explained as the "ring stain" of the current out-flying methane-ice mixture fragments (driven by the expansion of methane-evap-line, or the solar wind stop line). Using the probability functions in r- and θ-dimensions, we calculated out that Asteroid belt at n=48 has the probability peak range = 2.7 ±0.6 AU with the collective orbits' inclination range < 17.8 degree, and the cold-KBO at n=192 has the probability peak range = 43 ±5 AU with the collective orbits' inclination range < 8.9 degree. They fit to the Asteroid belt's and the cold-KBO's experimental data perfectly. A new concept has been proposed: Eigen quantum number n' is the maximum n' that can describe one orbit space's > 90% mass in a single |nLL> = |n',n'-1,n'-1> QM state. So n=48 and n=192 are the Eigen n for Asteroid belt and the cold-KBO. Using the Eigen n, the four undiscovered {3,n=2..5//6} belts (if they did not form planets)'s r ± Δr and Δθ' ranges are also predicted to be 173 ±13 AU, 390 ±25 AU, 693 ±38 AU, and 1081 ±53 AU, and 6.3 degree, 5.1 degree, 4.4 degree, and 4.0 degree, respectively.

References

[1] Yi Cao, SunQM-1: Quantum mechanics of the Solar system in a {N,n//6} QM structure. http://vixra.org/pdf/1805.0102v2.pdf （original submitted on 2018-05-03）

[2] Yi Cao, SunQM-1s1: The dynamics of the quantum collapse (and quantum expansion) of Solar QM {N,n} structure. http://vixra.org/pdf/1805.0117v1.pdf （submitted on 2018-05-04）

[3] Yi Cao, SunQM-1s2: Comparing to other star-planet systems, our Solar system has a nearly perfect {N,n//6} QM structure. http://vixra.org/pdf/1805.0118v1.pdf （submitted on 2018-05-04）

[4] Yi Cao, SunQM-1s3: Applying {N,n} QM structure analysis to planets using exterior and interior {N,n} QM. http://vixra.org/pdf/1805.0123v1.pdf （submitted on 2018-05-06）

[5] Yi Cao, SunQM-2: Expanding QM from micro-world to macro-world: general Planck constant, H-C unit, H-quasi-constant, and the meaning of QM. http://vixra.org/pdf/1805.0141v1.pdf （submitted on 2018-05-07）

[6] Yi Cao, SunQM-3: Solving Schrodinger equation for Solar quantum mechanics {N,n} structure. http://vixra.org/pdf/1805.0160v1.pdf （submitted on 2018-05-06）

[7] Yi Cao, SunQM-3s1: Using 1st order spin-perturbation to solve Schrodinger equation for nLL effect and pre-Sun ball's disk-lyzation. http://vixra.org/pdf/1805.0078v1.pdf （submitted on 2018-05-02）

[8] Yi Cao, SunQM-3s2: Using {N,n} QM model to calculate out the snapshot pictures of a gradually disk-lyzing pre-Sun ball. http://vixra.org/pdf/1804.0491v1.pdf （submitted on 2018-04-30）

[9] Yi Cao, SunQM-3s3: Using QM calculation to explain the atmosphere band pattern on Jupiter (and Earth, Saturn, Sun)'s surface. http://vixra.org/pdf/1805.0040v1.pdf （submitted on 2018-05-01）

[10] SunQM-3s6: Predict mass density r-distribution for Earth and other rocky planets based on {N,n} QM probability distribution. http://vixra.org/pdf/1808.0639v1.pdf (submitted on 2018-08-29)

[11] SunQM-3s7: Predict mass density r-distribution for gas/ice planets, and the superposition of {N,n//q} or |qnlm> QM states for planet/star. http://vixra.org/pdf/1812.0302v1.pdf (original submitted on 2018-12-17)

[12] SunQM-3s8: Using {N,n} QM to study Sun's internal structure, convective zone formation, planetary differentiation and temperature r-distribution. http://vixra.org/pdf/1808.0637v1.pdf (submitted on 2018-08-29)

[13] SunQM-3s9: Using {N,n} QM to explain the sunspot drift, the continental drift, and Sun's and Earth's magnetic dynamo. http://vixra.org/pdf/1812.0318v2.pdf (original submitted on 2018-12-18)

[14] SunQM-3s4: Using {N,n} QM structure and multiplier n' to analyze Saturn's (and other planets') ring structure. . http://vixra.org/pdf/1903.0211v1.pdf (submitted on 2019-03-11)

[15] Copied from wiki "Asteroid belt". Author: Piotr Deuar - http://en.wikipedia.org/wiki/Image:Main_belt_i_vs_a.png. Copy right: CC BY-SA 3.0. Created: 19 February 2006.

[16] Copied from wiki "Kuiper belt". "Distribution of cubewanos (or The Classical Kuiper belt object, blue), Resonant trans-Neptunian objects (red), Sednoids (yellow) and scattered objects (grey)". Author: Renerpho. Copy right: CC BY-SA 4.0. Created:14 October 2018.

[17] PBS-NOVA TV program "The Planets: Jupiter", https://www.pbs.org/video/the-planets-jupiter-dokro5/, at 23:54 / 53:17. (Aired 07/13/2019)

[18] PBS-NOVA TV program "The Planets: Inner worlds", https://www.pbs.org/video/the-planets-inner-worlds-jhasvd/ (Aired 07/24/2019). PBS-NOVA TV program "The Planets: Mars", https://www.pbs.org/video/the-planets-mars-qjisjr/ (Aired 07/24/2019).

[19] Darby Dyar, Suzanne E. Smrekar, and Stephen R. Kane, "The exoplanet next door". Scientific American, Feb. 2019, pp56.

[20] A series of my papers that to be published (together with current paper):
SunQM-3s10: Using {N,n} QM's Eigen n to constitute Asteroid/Kuiper belts, and Solar {N=1..4,n} region's mass density r-distribution and evolution.
SunQM-3s11: Using {N,n//q} QM's probability density 3D map to build a complete Solar system with time-dependent orbital movement.
SunQM-4: Using {N,n} QM to explain how planets are formed through accretion.
SunQM-4s1: Addendums, Updates and Q/A for SunQM series papers
SunQM-3s5: Using {N,n} QM structure and n*l*0 effect to analyze the bipolar outflow.
SunQM-5: A new version of QM based on interior {N,n}, multiplier n', |R(n,l)|^2 * |Y(l,m)|^2 guided mass occupancy, and RF, and its application from string to universe (drafted in April 2018).
SunQM-5s1: White dwarf, neutron star, and black hole re-analyzed by using the internal {N,n} QM (drafted in April 2018).

[21] Major QM books, data sources, software I used for this study are:
Douglas C. Giancoli, Physics for Scientists & Engineers with Modern Physics, 4th ed. 2009.
David J. Griffiths, Introduction to Quantum Mechanics, 2nd ed., 2015.
John S. Townsed, A Modern Approach to Quantum Mechanics, 2nd ed., 2012.
Stephen T. Thornton & Andrew Rex, Modern Physics for scientists and engineers, 3rd ed. 2006.
James Binney & David Skinner, The Physics of Quantum Mechanics, 1st ed. 2014.
Wikipedia at: https://en.wikipedia.org/wiki/
Online free software: WolframAlpha (https://www.wolframalpha.com/)
Online free software: MathStudio (http://mathstud.io/)
Offline free software: R
Microsoft Excel, Power Point, Word.
Public TV's space science related programs: PBS-NOVA, BBC-documentary, National Geographic-documentary, etc.
Journal: Scientific American.